Rho-mediated MRTF and YAP1 activation contributes to BRAF inhibitor resistance in Sox9^{High}/Sox10^{Low} melanoma cells.

Misek SA[1], Appleton KM[2], Dexheimer T[2], Lisabeth EM[2], Lo RS[3], Larsen SD[4], Gallo KA[1], Neubig RR[2,ψ]

[1]Department of Physiology, Michigan State University, East Lansing, MI, 48824, USA
[2]Department of Pharmacology, Michigan State University, East Lansing MI, 48824, USA
[3]Division of Dermatology, Department of Medicine, University of California, Los Angeles, California, 90095, USA; Department of Molecular and Medical Pharmacology, University of California, Los Angeles, CA 90095, USA; Jonsson Comprehensive Cancer Center, University of California, Los Angeles, CA 90095, USA; David Geffen School of Medicine, University of California, Los Angeles, CA 90095, USA.
[4]Department of Medicinal Chemistry, University of Michigan, Ann Arbor, Michigan, 48109, USA; Vahlteich Medicinal Chemistry Core, University of Michigan, Ann Arbor, Michigan, 48109, USA

Running title: RhoA-activated transcription in melanoma BRAFi resistance

Keywords: BRAF inhibitor; resistance; RhoA; MRTF; YAP1; Melanoma

Financial support: MSU Gran Fondo Skin Cancer Research Fund (RRN), NIH R01 AR066049 (SDL), MSUFCU Aitch Foundation Fellowship (SAM)

ψ *Corresponding author:* R.R. Neubig, MD, Ph.D., Michigan State University
Tel: 517-353-7145
Email: rneubig@msu.edu
Address: 1355 Bogue Street, B440 Life Sciences Building, East Lansing, MI, 48824

Abstract

Over half of cutaneous melanoma tumors have $BRAF^{V600E/K}$ mutations. Acquired resistance to BRAF inhibitors (BRAFi) remains a major hurdle in attaining durable therapeutic responses. In this study we demonstrate that approximately 50-60% of melanoma cell lines with acquired vemurafenib resistance activate the RhoA family signaling pathway. $RhoA^{High}$ BRAFi-resistant cells are sensitive to the combination of ROCK inhibitors and vemurafenib. Further, these $RhoA^{High}$ cells have >100-fold increase in Sox9 expression and >100-fold decrease in Sox10 expression. Two transcriptional co-activators downstream of RhoA, MRTF and YAP1, are activated in $Sox9^{High}/Sox10^{Low}$ BRAFi-resistant cells. Pharmacological inhibition of these transcriptional mechanisms re-sensitizes the cells to vemurafenib. Analysis of human BRAFi-resistant tumors reveals that many resistant tumors show gene expression signatures consistent with increased RhoA activation or activation of the transcriptional co-activators MRTF and YAP1. A subset of melanoma tumors in the TCGA dataset with low Sox10 expression also have elevated RhoA, MRTF, and YAP1 activation signatures. Taken together, these results support the concept of targeting RhoA-regulated gene transcription pathways as a promising approach for treating or preventing BRAFi-resistance in melanoma.

Introduction:

Most cutaneous melanoma tumors have $BRAF^{V600}$ mutations (1). This results in constitutive BRAF activity and downstream MAPK pathway activation, independent of upstream stimuli. BRAF inhibitors in combination with MEK inhibitors was proposed to overcome BRAF inhibitor resistance (Nazarian et al, Nature 2010) and clinically is superior to BRAF inhibitor monotherapy against $BRAF^{V600}$-mutant tumors (2-4). However, acquired resistance to the BRAF and MEK inhibitor combination is still common (5), consistent with MAPK pathway-redundant resistance mechanisms as important clinically (6, 7). Several resistance mechanisms have been identified which result in MAPK pathway reactivation, such as NRAS mutation or BRAF alternative

splicing (6, 8-12). These MAPK-reactivating alterations only explain ~50% of BRAFi-resistance mechanisms (5) (7). Some MAPK-redundant resistance mechanisms result from cancer cell intrinsic, epigenomically driven, adaptive responses to drug pressure early during therapy (6) and likely result in wide-ranging phenotypic switches in melanoma with acquired MAPK inhibitor resistance in patients who relapse of such therapies (7). Melanoma cells grown without drug pressure stochastically switch between a rapid-cycling cell state and a rare slow-cycling cell state (13). Treatment with a BRAF inhibitor selects for cells in the slow cycling state (6, 12). These data are further supported by the observation that BRAFi/MEKi-resistant cells and tumors can be re-sensitized to treatment with BRAF or MEK inhibitors after a "drug holiday" (14-16).

The RhoA subfamily (RhoA, RhoB, and RhoC) GTPases act as molecular switches which regulate actin dynamics. In this report, we will use RhoA to refer to the whole subfamily. In melanoma, the RhoA subfamily promotes invasion and metastasis (17-19), and inhibition of RhoA signaling suppresses tumor growth (20). RhoB is upregulated upon short-term vemurafenib treatment, and RhoB silencing sensitizes cells to BRAF and MEK inhibitors (21). Canonically, RhoA GTPases promote the formation of actin stress fibers by promoting G-actin polymerization and inhibiting F-actin depolymerization (22-24). Actin stress fibers are increased in melanoma cells with acquired BRAFi resistance (25).

In addition to regulating actin dynamics, RhoA GTPases also regulate gene transcription. This is, in part, through actin polymerization-dependent activation of MRTF and YAP1. MRTF and YAP1 are transcriptional co-activators which, upon activation, translocate into the nucleus and regulate gene transcription. Silencing of MRTF or SRF, a transcription factor by which MRTF modulates gene expression, prevents melanoma metastasis (26). Previously, we have developed a series of MRTF-pathway inhibitors including CCG-203971 and CCG-222740 (27-29). We have demonstrated that CCG-203971 prevents melanoma metastasis, induces G1 cell cycle arrest, and reduces growth of melanoma cells (28). When bound to G-actin, MRTF is sequestered in the cytoplasm due to masking of the MRTF nuclear localization signal by G-actin. Upon RhoA-mediated F-

actin polymerization, the cytosolic G-actin pool is depleted resulting in MRTF dissociation from G-actin, and translocation into the nucleus (26, 30-33). YAP1 is also activated upon F-actin polymerization, but through a different mechanism (34-36). YAP1 has been shown to promote BRAFi/MEKi resistance in melanoma through suppression of apoptosis via BCL-xL and BIM dysgulation (7, 25, 37, 38), and positive enrichment/accumulation of YAP1 signature/protein has been documented in about 40% of clinical melanoma samples from patients who relapsed on MAPK inhibitor therapies (7)

Sox10 is a neural crest lineage transcription factor, which is highly expressed in melanocytes and some melanoma cells (39) and Sox10 loss has been associated with BRAFi inhibitor resistance. Melanoma cells with high Sox10 expression are more proliferative and Sox10 knockdown reduces melanoma cell proliferation (40-42). Interestingly, there is an inverse relationship between Sox10 expression and Sox9 expression and these two proteins reduce each other's expression (41). A subset of melanoma cells is in a transient slow-cycling, pre-drug-resistant state which are epigenetically poised to become drug-resistant (6, 13). Upon BRAFi treatment, these cells are transformed into a stable resistant state, which is initiated with loss of Sox10-mediated gene transcription, later followed by increased AP-1- and TEAD-mediated gene transcription. These findings highlight that Sox10 is lost early during the development of BRAFi resistance. Another study demonstrated that Sox10 silencing promotes BRAFi resistance, in part through activation of TGFβ signaling (43). Interestingly, TGF-β can indirectly activate RhoA (44, 45).

Previous studies have demonstrated that non-mutational, acquired resistance mechanisms represent a major hurdle in maintaining a durable response to MAPK-directed therapeutics (7). One major acquired resistance mechanism may be activation of the RhoA pathway. In this study we build upon existing literature to demonstrate that actin stress fiber accumulation and RhoA signaling is elevated in approximately half of vemurafenib-resistant melanoma cell lines tested and that this mechanism is also operational in clinical tumors. $RhoA^{High}$ but not $RhoA^{Low}$-resistant lines are partially resensitized to vemurafenib by two structurally distinct

ROCK inhibitors. We also demonstrate that in RhoA^{High} cells Sox9 is upregulated and Sox10 is downregulated, a pattern also seen in human tumor samples. A RhoA/C expression signature is inversely correlated with Sox10 expression in TCGA melanoma tumors or with a Sox10 signature applied to datasets from single cell RNA-Seq of melanoma tumors. We also find that Sox9^{High}/Sox10^{Low} BRAFi-resistant cells have increased MRTF and YAP1 activation; and pharmacological targeting of MRTF- and YAP1-mediated gene transcription re-sensitizes these BRAFi-resistant cells to vemurafenib.

Materials and Methods:

Cell lines and culture

Selection of Vemurafenib-resistant cells:

UACC62 and SK-Mel-19 cells were seeded into 10-cm tissue culture plates at ~30% confluence and grown in DMEM as described below. After the cells had adhered to the plate (~16 h), culture medium was supplemented with 2 µM vemurafenib. Medium was exchanged every 2-3 days for 10 mL of fresh media supplemented with 2 µM vemurafenib. Cells were split at a 1:3 ratio into a new 10-cm tissue culture plate when they reached ~75% confluence (approximately 3-4 weeks) and approximately weekly for each subsequent passage. After two months of selection, cell populations were expanded in vemurafenib-containing media and frozen.

Sources of cells:

Parental (P) and vemurafenib-resistant (R) M229P/R, M238P/R, and M249P/R cells were generously provided by Dr. Roger Lo at UCLA (8). SK-Mel-19 and UACC62 cells were obtained from Dr. Maria Soengas at The University of Michigan.

Cells were cultured in DMEM (Gibco #11995-065) supplemented with 10% FBS (Gibco #10437-028) and 1% Antibiotic-Antimycotic (ThermoFisher #15240062). Vemurafenib-resistant cells were continuously cultured in the presence of 2 µM vemurafenib. Cells were split at ~75% confluence. Vemurafenib was removed from the culture medium when cells were seeded for experiments (e.g. immunofluorescence staining or qRT-

PCR), except where otherwise indicated. Cells were routinely tested for mycoplasma contamination by DAPI staining. STR profiling on all cell lines was performed at the MSU genomics core. In all cases, isogenic pairs of cell lines had the same STR profile.

Compounds and Antibodies

Vemurafenib (#S1267), dabrafenib (#S2807), Y-27632 (#S1049), fasudil (#S1573), and dasatinib (#S1021) were purchased from Sellekchem. CCG-222740 (29) was synthesized in the lab of Dr. Scott Larsen at the University of Michigan. All compounds were diluted in DMSO to a stock concentration of 10 mM. Compounds were frozen at -20 ºC. Antibodies against YAP1 (#14074), MLC2 (#3672), pMLC2 (#3674), and Sox10 (#89356) were purchased from Cell Signaling. Antibodies against MRTF-A (#sc21558), MRTF-B (#sc98989), and Actin (#sc1616) were purchased from Santa Cruz. Donkey anti-Mouse800 (#926-32212), Donkey anti-Goat680 (#926-68074), and Donkey anti-Rabbit680 (#926-68073) immunoblotting secondary antibodies were purchased form LI-COR. Alexa Fluor goat anti-rabbit488 (#A11034) and donkey anti-goat488 (#A11055) were purchased from Invitrogen. Alexa Fluor546 Phalloidin (#A22263) was purchased from ThermoFisher.

qRT-PCR

Cells were cultured and treated as indicated, rinsed once in PBS, and total cellular RNA was harvested with the Qiagen RNeasy kit (#74104) according to the manufacturer's protocol. RNA was eluted in nuclease-free H_2O. cDNA was synthesized using the High-Capacity cDNA RT kit from ThermoFisher (#4368814) from 1000 ng of total RNA, according to the manufacturer's protocol. qPCR was performed using the SYBR Green PCR Master Mix (#4309155) from ThermoFisher according to the manufacturer's protocol using an Agilent Mx3000P qPCR instrument. Sox9 primers were purchased from Integrated DNA Technologies with the following sequences: Sox9 Forward (5'-AGCGAACGCACATCAAGAC-3'), Sox9 Reverse (5'-CTGTAGGCGATCTGTTGGGG-3'), Sox10 Forward (5'-CCTCACAGATCGCCTACACC-3'), Sox10 Reverse (5'-

CATATAGGAGAAGGCCGAGTAGA-3'). Primers were designed using the Harvard Primer Bank tool (https://pga.mgh.harvard.edu/primerbank/). Fold-change analysis was performed using the ΔΔCT method.

RNA-Seq sample preparation and data processing

Total cellular RNA was extracted from UACC62P and UACC62R cells (two biological replicates per cell line) using the same method which was used for qPCR experiments. RNA concentration was measured by Qubit and quality control was performed on an Agilent 2100 Bioanalyzer in the MSU Genomics Core. All RNA samples had a RIN score > 8. Barcoded libraries were prepared using the Illumina TruSeq Stranded mRNA Library Preparation Kit on a Perkin Elmer Sciclone G3 robot following manufacturer's recommendations. Completed libraries were QC'd and quantified using a combination of Qubit dsDNA HS and Caliper LabChipGX HS DNA assays. Libraries were pooled and run on two lanes, and sequencing was performed in a 1x50 bp single-end read format using HiSeq 4000 SBS reagents. Base calling was done by Illumina Real Time Analysis, RTA_ v2.7.7 and output of RTA was demultiplexed and converted to FastQ format with Illumina Bcl2fastq v2.19.0. Sequencing was performed at a depth of >30M reads/sample. Quality control was performed on the FastQ files using FastQC v0.11.5, and reads were trimmed using Trimmomatic v0.33. Reads were mapped using HISAT2 v2.1.0 and analyzed using HTSeq v0.6.1. Differential gene expression was calculated using edgeR. Raw RNA-Seq reads and processed HTSeq read counts are available on GEO under GSE115938.

Immunoblotting

Cells were cultured and treated as indicated, placed on ice, and rinsed once in cold PBS. Cells were lysed in 2x Laemmli Sample Buffer (Biorad, #1610737). Samples were sonicated with a probe sonicator for approximately 5 sec, then boiled at 100 ºC for 10 min. Samples were loaded onto a 12% polyacrylamide gel and transferred to Immobilon-FL PVDF Membrane (Millipore Sigma, #IPFL00010). Membranes were blocked in 5% BSA + TBS-Tween (1:1000) for 1 h, then incubated in primary antibody overnight at 4 ºC. Membranes were washed 3x

in TBS-Tween and were then incubated in the appropriate secondary antibody at a 1:20,000 dilution for 1 h at room temperature. All antibodies were diluted in blocking buffer. Membranes were washed 3x in TBS-Tween then dried and imaged on a LI-COR Odyssey FC imaging system.

Immunofluorescence staining

Cells were seeded into 8-well chamber slides and were treated as indicated in the figure legends. Cells were fixed with 3.7% formaldehyde for 15 min then blocked in 2% BSA PBS-Triton (0.1%) for 1 h at room temperature. Cells were incubated overnight at 4 ºC in primary antibody at a 1:100 (MRTF-A or MRTF-B) or 1:500 (YAP1) dilution in blocking buffer. Cells were washed 3x in PBS then were incubated in the appropriate secondary antibody at a 1:1000 dilution for 1 h at room temperature. Cells were washed 3x in PBS then were mounted in ProLong Gold Antifade + DAPI (ThermoFisher, #P36935). Slides were cured overnight at room temperature and were then imaged on a Nikon TE2000-U Fluorescence Microscope at 20x magnification.

Cells were stained with Alexa Fluor546 Phalloidin (#A22263) to visualize F-Actin. For these experiments, cells were fixed and blocked as described above. Cells were then incubated in Phalloidin diluted 1:100 in blocking buffer for 1 h at room temperature before being washed and mounted. For all immunofluorescence experiments, images were blinded by an independent party or an automated R script before quantification. For a cell to be considered as stress fiber-positive, the cell was required to contain at least one stress fiber which spanned >90% the length of the cell.

Cell viability experiments

Cells were seeded into 384-well tissue culture plates (PerkinElmer, #6007689) at a density of 1000 cells/well in 20 uL of media and were allowed to attach overnight. The next day, drugs were pre-diluted at 4x final concentration in culture medium then added to the 384-well plates so that the final volume was 40 µL/well. A PBS barrier was added to the outer wells of the plate to limit evaporation. Cells were cultured under these conditions for 72 h. To assess viability, 10 µL of CellTiter-Glo (Promega, #G7573) was added to each well.

Plates were incubated for 5 min at room temperature then briefly centrifuged (4000 rpm, 60 seconds) before being read on a Bio-Tek Synergy Neo plate reader. Data are plotted versus Vemurafenib concentration for each treatment condition. The Area Under the Curve (AUC) was calculated for each curve using GraphPad Prism.

Bioinformatics

Dataset Processing

Cancer Cell Line Encyclopedia (CCLE) gene expression Affymetrix CEL files (Version 19-Mar-2013) were downloaded from the Broad Institute CCLE data portal. CEL files were processed using Affymetrix Expression Console (Build 1.4.0.38). Probe IDs were collapsed to gene names using the CollapseDataset function on GenePattern. The TCGA RNA-Seq dataset for cutaneous melanoma (SKCM) was downloaded from the UCSC Cancer Genome Browser portal. No further data processing was performed prior to analysis.

RNA-Seq data for 62 human tumors paired for pre- and post- MAPK inhibitor resistance was downloaded from GSE65185 (7). Analysis of these data was performed on the pre-processed CuffnormFPKM dataset included in this series. RNA-Seq data for *in vitro* generated vemurafenib-resistant M229P/R and M238P/R cells was downloaded from GSE75313 (6). These data were processed using the above described RNA-Seq data processing pipeline.

Gene Ontology/KEGG pathway analysis

Using the CCLE dataset, 38 adherent cell lines with $BRAF^{V600}$-mutations were identified. For all cell lines, PLX4720 (activity area) was correlated with gene expression. Genes highly expressed in resistant cells (genes with a Pearson correlation coefficient < -0.5 when correlated with PLX4720 sensitivity) and genes weakly expressed in resistant cells (Pearson correlation coefficient > 0.5) were identified. Gene ontology and KEGG pathway analysis was performed on the gene sets using GATHER (http://changlab.uth.tmc.edu/gather/gather.py) with network inference.

GSEA/ssGSEA

GSEA (v19.0.24) was performed using GenePattern (http://software.broadinstitute.org/cancer/software/genepattern/) with 'number of permutations' = 1000, and 'permutation type' = phenotype. All other parameters were left as default. ssGSEA (9.0.9) was performed on GenePattern with all parameters left as default. The ssGSEA output values were z-score normalized.

A RhoA/C gene signature was generated by using all genes which are upregulated > 2-fold by overexpression of either RhoA or RhoC from the GSE5913 dataset in NIH-3T3 cells. These two lists were merged, and duplicates were removed. This resulted in a list of 79 genes (Supplemental Table 1).

A Sox10 gene signature was created using the 96 h gene expression data in GSE37059 in M010817 cells. The 214 genes downregulated > 2-fold when Sox10 expression was knocked down were taken as the Sox10 signature (Supplemental Table 1). Following ssGSEA and z-score normalization, the sign of the signature score was inverted so that a positive signature score indicates high predicted Sox10 activity and a negative signature score indicates low predicted Sox10 activity.

Differential gene expression between the vemurafenib-sensitive and resistant pairs UACC62P/R, M229P/R, and M238P/R was calculated using the edgeR package. The top 500 differentially expressed genes for each cell line pair were stratified into lists of upregulated and downregulated genes. The intersection of all upregulated or downregulated genes among the three cell lines was determined resulting in 54 genes which were downregulated in all three resistant cell lines ('Downregulated_In_Resistant' signature) and 34 genes that were upregulated in all three resistant cell lines ('Upregulated_In_Resistant' signature) (Supplemental Table 1).

The YAP1 signature used was the CORDENONSI_YAP_CONSERVED_SIGNATURE in the C6 collection on MSigDB. The MRTF signature is comprised of all genes downregulated > 2-fold upon MRTF knockdown in B16F2 melanoma cells (26) (Supplemental Table 1).

Drug Response Signatures

Gene expression profiling and drug IC50s were downloaded from the GDSC data portal (https://www.cancerrxgene.org/downloads). Gene expression data was median centered so that the median expression of each gene was equal to 0. Data was randomly divided into a training (80%) and test (20%) set. A predictive model was built on the training set for each compound (n = 265 compounds) using a random forest algorithm (randomForest package in R) with ntrees = 500 and mtry = sqrt(#genes). Each model was validated on the test dataset by calculating the Pearson correlation coefficient between the predicted and actual IC50s. Models with a Pearson correlation coefficient > 0.3 were considered predictive. A full table of these results is included as (Supplemental Table 2). To use gene expression data to predict drug response on clinical tumors, the TCGA SKCM data were median-centered using the same method used on the GDSC training data. Since the TCGA and GDSC datasets were collected on different gene expression analysis platforms, the two datasets were filtered to include only overlapping genes. Models from GDSC which were deemed predictive for a drug response were then projected onto the TCGA dataset. TCGA samples were stratified by Sox10 expression ($Sox10^{Low}$ = Sox10 expression is >1 SD below mean, $Sox10^{High}$ = Sox10 expression is all other samples). The average predicted IC_{50} for the $Sox10^{Low}$ and $Sox10^{High}$ tumors was calculated by averaging the predicted $\log(IC_{50})$ for each sample class.

Statistical Analysis

Most bioinformatics analysis was performed using R v3.3.0. Data analysis and statistics were performed using GraphPad Prism v6 or v7. Dose response curves were fit using nonlinear least square regression [log(agonist) vs. response – Variable slope (four parameters)]. The AUC was calculated for each dose response curve in

GraphPad Prism over a vemurafenib concentration range of 10^{-9} to 10^{-5}. Datasets with two samples per group were analyzed by unpaired two-tailed t-tests. Pearson correlation coefficients were calculated in R (for drug response signatures) or GraphPad Prism (for all other analysis). Data are presented as mean ± S.E.M, and a p-value < 0.05 was considered statistically significant.

Figure 1. RhoA is activated in BRAFi-resistant melanoma cells and tumors. A) Cells were seeded into 8-well chamber slides and were allowed to attach overnight. The next day cells were fixed and stained with fluorescently labeled phalloidin. Representative images from n = 3 biological replicates and n = 1 technical replicates. **B)** Actin stress fiber positive cells were quantified using ImageJ. Statistical analysis was performed using unpaired t-tests. **C)** $MLC2^{S18/19}$ phosphorylation in UACC62 (left) and SK-Mel-19 (right) parental and resistant cells was assessed by immunoblotting. Total MLC2 and Actin were used as loading controls. Representative blots from n = 3 biological replicates and n = 1 technical replicates. **D)** KEGG pathway analysis of genes significantly positively (Pearson correlation coefficient > 0.5) or negatively (Pearson correlation coefficient < -0.5) correlated with PLX4720 response in 38 $BRAF^{V600}$-mutant CCLE cell lines. **E)** A RhoA/C signature was correlated with PLX4720 sensitivity using ssGSEA on 38 $BRAF^{V660}$-mutant CCLE cell lines. **F)** Gene ontology of genes significantly positively (Pearson correlation coefficient > 0.5) or negatively (Pearson correlation coefficient < -0.5) correlated with PLX4720 response in 38 $BRAF^{V600}$-mutant CCLE cell lines. **G)** RhoA/C activation was predicted from the gene expression profiles from paired human melanoma tumors pre- and post-BRAFi/MEKi resistance using ssGSEA. Tumors were stratified into those with increased predicted RhoA/C activation (n = 24) or decreased RhoA/C activation (n = 17)

Figure 2. ROCK inhibition reverses BRAFi resistance in RhoA^{High} BRAFi-resistant melanoma cells. Parental and Vemurafenib-resistant cell lines were seeded into 384-well plates at a density of 1,000 cells/well and cells were allowed to attach overnight. The next day, cells were treated with Vemurafenib at the indicated concentrations with or without the ROCK inhibitors Y-27632 (red) or Fasudil (blue) at 10 µM. Cells were grown for 72 h then viability was measured with CellTiter-Glo. Pooled viability data from n = 3 biological replicates and n = 1 technical replicates. **A-H)** Cell lines were treated as labeled with ROCK inhibitors (Y-27632 or Fasudil) along with Vemurafenib. **I)** Schematic of Area Under Curve (AUC) calculation. Larger AUC indicates lower sensitivity to the drug combination and smaller AUC indicates greater sensitivity to the drug combination. **J)** Heatmap of AUC values for the Vemurafenib/Y-27632 drug combination for four parental and resistant cell line pairs. **K)** Heatmap of AUC values for the Vemurafenib/Fasudil drug combination for four parental and resistant cell line pairs.

Figure 3. Sox10 is downregulated and Sox9 is upregulated in a subset of Vemurafenib-resistant cells. A) RNA-Seq was performed on parental (UACC62P) and Vemurafenib-resistant (UACC62R) cells. Differential gene expression was visualized on a volcano plot. n = 2 biological replicates and n = 1 technical replicates per treatment condition. **B)** Sox9 and Sox10 mRNA expression was assessed by qRTPCR across a panel of 5 parental and Vemurafenib-resistant cell line pairs. Pooled qPCR data from n = 3 biological replicates and 1-3 technical replicates. **C)** Sox10 protein expression was assessed across a panel of 4 parental and resistant melanoma cell lines. Actin was used as a loading control. Representative image from n = 3 biological replicates

and n = 1 technical replicates. **D)** The tumor samples in the TCGA SKCM RNA-Seq dataset (n = 473) were stratified into Sox10^{Low} (> 1 SD below mean, 17 samples) or Sox10^{High} tumors. **E)** Sox9 mRNA expression in the TCGA SKCM RNA-Seq dataset was compared between the samples stratified by Sox10 expression. **F)** RhoA/C activation was predicted on TCGA SKCM tumors using ssGSEA with our RhoA/C gene signature. Tumors were stratified based on Sox10 expression. **G)** Correlation of a RhoA/C signature and a Sox10 signature on single cell RNA-Seq data (46) from melanoma cells isolated from human tumors using ssGSEA. **H)** Drug signatures for 265 common anti-cancer drugs in the GDSC dataset were generated using the random forest algorithm. These signatures were projected onto the TCGA SKCM RNA-Seq dataset and predicted drug sensitivity for each tumor was calculated. Tumors were stratified by Sox10 expression and selectivity was calculated by measuring the fold change in signature score between Sox10^{Low} and Sox10^{High} tumors. **I)** Schematic of how the 'Upregulated_In_Resistant' and 'Downregulated_In_Resistant' gene sets were generated. **J)** GSEA using the 'Upregulated_In_Resistant' and **K)** 'Downregulated_In_Resistant' gene sets on the TCGA SKCM RNA-Seq dataset, stratified by Sox10 expression.

Figure 4. YAP1 and MRTF-A are activated in Sox10^{Low} BRAFi-resistant cells. A) M229P/R, M238P/R, and UACC62P/R cells were seeded into 8-well chamber slides and were allowed to attach overnight. The next day, cells were fixed and stained with an anti-YAP1 or anti-MRTF-A antibodies. Representative images from n = 3 biological replicates and n = 1 technical replicates. **B)** Quantification of staining from panel 'A'. **C)** Multiple YAP1/MRTF-associated genes are highly expressed in PLX4720-resistant cells. **D)** A YAP1 signature was projected onto the TCGA SKCM RNA-Seq dataset using ssGSEA. Samples were stratified by Sox10 expression (see fig 1D). Statistical analysis was performed with an unpaired t-test. **E)** A MRTF signature was projected onto the TCGA SKCM RNA-Seq dataset using ssGSEA. Samples were stratified by Sox10

expression (see fig 1D). Statistical analysis was performed with an unpaired t-test. **F)** MRTF and YAP1 signatures were predicted for human melanoma tumor pairs which had an increase in RhoA/C signature score from Fig. 1G. Change in MRTF and YAP1 signature score between baseline and resistant tumors is plotted.

Figure 5. Dasatinib and CCG-222740 reverse BRAFi-resistance. A) Cells were seeded into 8-well chamber slides and were allowed to attach overnight. The next day, cells were treated with Dasatinib (500 nM) for 16 h, then cells were fixed and stained with an anti-YAP1 antibody. Representative images from n = 3 biological replicates and n = 1 technical replicates. **B)** Quantification of YAP1 localization from panel "A". **C-J)** Parental and Resistant cell lines were seeded into 384-well plates at a density of 1,000 cells/well and cells were allowed to attach overnight. The next day, cells were treated in dose response with Vemurafenib at the indicated concentrations -/+ Dasatinib (red) or CCG-222740 (blue) at 10 µM. At 72 h viability was measured with CellTiter-Glo. Cells and treatments were as indicated with Dasatinib or the MRTF pathway inhibitor CCG-222740. Dose response curves are viability data are from n = 3 biological replicates and n = 1 technical replicates. **K)** Heatmap of AUC values for the Vemurafenib/Dasatinib drug combination for four parental and resistant cell line pairs. **L)** Heatmap of AUC values for the Vemurafenib/CCG-222740 drug combination for four parental and resistant cell line pairs.

Results:

RhoA activation in BRAFi-resistant melanoma cells and tumors. We generated vemurafenib-resistant melanoma cells by exposing them to vemurafenib (2 μM). After two months, this resulted in a population of cells that grew well in the presence of vemurafenib. One of the resistant cell lines (UACC62R) had a flattened morphology when compared to the parental cell line, while a different cell line (SK-Mel-19R) displayed no obvious morphological changes from its parental counterpart. Since cell shape is largely controlled through modulation of the actin cytoskeleton, we examined F-actin structure by staining the cells with fluorescently labeled phalloidin. UACC62R cells showed a marked increase in actin stress fiber positive cells compared to the parental line, while there was no effect in SK-Mel-19R cells compared with parental control cells **(Fig. 1A)**. We then expanded this panel to include three other vemurafenib-resistant cell line pairs (M229, M238, and M249) which were previously generated using similar methods (8). Two of the three resistant cell lines (M229R, and M238R) showed an increase in actin stress fibers similar to our observations in UACC62R cells, while M249R cells had no change in actin stress fiber-positive cells **(Fig. 1B).** Actin stress fibers are primarily controlled by RhoA family activation. Another readout of RhoA activation is MLC2 phosphorylation and $pMLC2^{S18/19}$ is increased in UACC62R (actin stress fiber-positive) cells, but not in SK-Mel-19R (actin stress fiber-negative) cells **(Fig. 1C)**. Taken together, these data showed that the RhoA pathway is activated in a 3 of 5 vemurafenib-resistant cells.

To more broadly confirm this finding, we correlated sensitivity to PLX4720 (a BRAF inhibitor which is structurally similar to vemurafenib) with the gene expression results of 38 $BRAF^{V600}$-mutant cell lines from the Cancer Cell Line Encyclopedia (CCLE). Genes which are highly expressed in PLX4720-resistant cells (genes with a Pearson correlation of gene expression values vs drug activity area < -0.5) were analyzed by Gene Ontology and KEGG pathway analysis. One of the most statistically significant GO terms was “small GTPase mediated signal transduction” **(Fig. 1D)** and the most statistically significant KEGG pathway was “Regulation of actin cytoskeleton” **(Fig. 1E)**. A RhoA/C gene signature is also inversely correlated (R = 0.42) with PLX4720 sensitivity **(Fig. 1F)**. Collectively, these data suggest that our phenotypic observations are more

broadly applicable in a wider panel of cell lines and that RhoA activation is positively correlated with BRAFi resistance.

To determine whether these cell line observations are applicable in the clinical context, we analyzed RNA-seq data from 41 tumors before and after development of resistance to BRAFi/MEKi (7). More than half of the resistant tumors (n = 24) had an increased RhoA/C signature score over the baseline tumor **(Fig. 1G)**. Taken together, these data suggest that RhoA is activated in approximately half of BRAFi-resistant cells and tumors, and that RhoA activation is inversely correlated with BRAFi sensitivity.

ROCK inhibition sensitizes RhoA^{High} BRAFi-resistant melanoma cells. It is difficult to pharmacologically target RhoA directly, so an alternative approach is to target downstream effector pathways. To this end, we used two ROCK inhibitors, Y-27623 and Fasudil, with structurally distinct chemical scaffolds. Cells were profiled in 12-point concentration response studies with vemurafenib with or without Y-27632 or Fasudil. Neither ROCK inhibitor significantly sensitizes M229P cells to vemurafenib **(Fig. 2A/E)**, but both markedly re-sensitize the RhoA^{High} M229R cells to vemurafenib **(Fig. 2B/F)**. In contrast, no re-sensitization is observed in the RhoA^{Low} vemurafenib-resistant M249R cells **(Fig. 2D/H)**. These data are consistent with the observation that M229R cells are actin stress fiber positive, while M249R cells are actin stress fiber negative. To more quantitatively measure this phenotype, we calculated the Area Under the Curve (AUC) of each dose response curve **(Fig. 2I)**. This is a more comprehensive approach to measure the effect of the drug combination since this measurement is sensitive to changes in both IC_{50} and E_{max}. All three actin-stress-fiber positive resistant lines were re-sensitized to vemurafenib by either Y-27632 **(Fig. 2J)** or Fasudil **(Fig. 2K)**, however, neither ROCKi re-sensitizes M249R (actin stress fiber-negative) cells. Taken together, these results indicate that ROCK inhibition selectively re-sensitizes RhoA^{High} vemurafenib-resistant cells, but not RhoA^{Low} cells.

Sox9/Sox10 expression switch in RhoA^{High} vemurafenib-resistant cells. We next wanted to understand mechanistically why the RhoA pathway is only activated in a subset of vemurafenib-resistant cells. We performed RNA-seq on UACC62P/R cells and found that a number of genes involved in melanocyte differentiation and melanoma biology including TYR, POSTN, WNT5A, AXL, SOX9, SOX10, and several collagen isoforms were up- or down-regulated. Among these, SOX10 is one of the most significantly downregulated genes in UACC62R cells **(Fig. 3A)**. Sox10 has been previously linked to vemurafenib resistance in a mechanism that is partially dependent on TGFβ-pathway activation (43) and as a part of an epigenome-driven transcriptomic reprogramming (6). We also discovered that Sox9 is one of the most significantly upregulated genes in UACC62R cells **(Fig. 3A)**. Since Sox9 and Sox10 expression levels are reportedly mutually antagonistic (41), we wanted to determine whether the inverse relationship between Sox9 and Sox10 expression is observed in BRAFi-resistant melanoma cells. This finding also held up in a larger panel of cell lines. Of the five tested, only the three cell lines with RhoA activation show upregulated Sox9 and downregulated Sox10 **(Fig. 3B)**. This result also holds true at the protein level; Sox10 is downregulated in UACC62R, M229R, and M238R cells, but not in M249R cells **(Fig. 3C)**. To extend these observations to clinical melanomas, we stratified SKCM tumors in the TCGA RNA-Seq dataset into Sox10^{Low} (> 1 SD below mean expression) and Sox10^{High} tumors (all others) **(Fig. 3D)**. The Sox10^{Low} tumors (n = 17) have significantly increased Sox9 expression, demonstrating that the inverse relationship we observe in BRAFi-resistant cell lines also extends to human melanoma tumors **(Fig. 3E)**. The small number of Sox10^{Low} tumors may be due to the fact that the tumors the TCGA SKCM dataset are BRAFi/MEKi-treatment naïve. Sox10^{Low} TCGA tumors also have increased RhoA/C gene signature enrichment scores **(Fig. 3F)**. We then assessed RhoA/C and Sox10 activation signatures on the single cell level using a melanoma single cell RNA-Seq dataset (46). It was necessary to use a Sox10 signature instead of Sox10 expression itself due to the low sequence coverage in single cell sequencing experiments. There is a strong inverse correlation between Sox10 activation and RhoA/C activation signatures **(Fig. 3G)**.

We then wanted to identify drugs that selectively target Sox10^{Low} tumors, since this would give insight into the signaling pathways activated in these cells and would identify potential therapeutics which could be used to reverse or prevent BRAFi-resistance. We generated gene expression signatures to predict drug response for 265 common anti-cancer drugs. Then we projected these signatures onto the TCGA dataset to find drugs that are predicted to selectively target Sox10^{Low} tumors. Four of the top six drugs predicted to be selective for Sox10^{Low} cells inhibit either ROCK or SRC. These drugs are GSK269963 (ROCKi), Y-39983 (ROCKi), GASK269962 (SRCi), and Dasatinib (SRCi) **(Fig. 3H)**. To confirm that the Sox10^{Low} TCGA tumors are phenotypically similar to Sox10^{Low} vemurafenib-resistant cells, we generated gene signatures "Upregulated_In_Resistant" and "Downregulated_In_Resistant" to include genes that are upregulated or downregulated in M229R, M238R, and UACC62R cells compared to their parental lines before selection. The gene set which is highly expressed in drug-resistant cells is enriched in Sox10^{Low} TCGA tumors. Conversely, the genes which are down-expressed in drug-resistant cells are enriched in Sox10^{High} TCGA tumors. Taken together, these data demonstrate that Sox10^{Low} TCGA tumors are very similar on a transcriptional level to the Sox10^{Low} BRAFi-resistant cells studied here (**Fig. 3I)**. While only 17/473 of the tumors in the TCGA SKCM dataset have low Sox10 expression, these tumors were never selected with BRAFi/MEKi, which may explain the low prevalence of tumors with this transcriptional profile. Further, this suggests that low Sox10 expression or the related transcriptomic phenotype(s) could be responsible for intrinsic resistance in addition to acquired resistance in a subpopulation of patients.

MRTF and YAP activation in RhoA^{High} BRAFi-resistant cells. In addition to modulating cytoskeletal re-arrangement, RhoA also regulates gene expression. Two transcriptional co-activators downstream of RhoA are YAP1 and MRTF. RhoA-mediated F-actin polymerization results in the nuclear translocation and transcriptional activation of YAP1 and MRTF. MRTF and YAP1 have similar transcriptional outputs and can perform redundant functions in several contexts (47, 48). To determine whether YAP1 and MRTF are activated in RhoA^{High} BRAFi-resistant cells, we measured the subcellular localization of YAP1 and MRTF-A/B **(Fig.**

4A/B). YAP1 nuclear localization is elevated in M229R and M238R cells. There is only a modest increase in nuclear YAP1 in UACC62R cells. Interestingly, MRTF-A nuclear accumulation is elevated in UACC62R cells, but not in M229R or M238R cells, and there were no major changes in MRTF-B localization in all three cell lines (data not shown). Several YAP1- and MRTF-related genes are highly expressed in innate BRAFi resistance **(Fig. 4C)**. These include the YAP1/MRTF target gene CYR61 and genes encoding proteins which activate RhoA (ARHGEF12, GNA11, GNA12, TGFβ1) as well as YAP1 and YES1.

To test whether YAP1 and MRTF are activated in human tumors, we determined/calculated YAP1 and MRTF signature activation in TCGA tumors. $Sox10^{Low}$ tumors have elevated YAP1 and MRTF signature gene expression **(Fig. 4D/E)**. YAP1 and MRTF activation was predicted on the paired pre- and post-resistance human melanoma tumors which had an increase in RhoA/C signature gene expression **(Fig. 4F)**. Out of this subset of tumors, only 3/24 displayed neither activation of YAP1 or MRTF target genes. Half (12/24) of the tumors had predicted activation of both YAP1 and MRTF, which could possibly result from the high degree of redundancy in the transcriptional output from YAP1 and MRTF or subpopulation heterogeneity. Some appeared to have selective activation of YAP or MRTF, which is interesting considering the apparent mutual exclusivity of MRTF-A/YAP1 activation in our cell line models **(Fig. 4A/B)**. Taken together, these data demonstrate that YAP1 and/or MRTF are activated in nearly all of the $Sox9^{High}/Sox10^{Low}$ BRAFi-resistant cells/tumors.

Pharmacologically targeting MRTF/YAP-mediated gene transcription. Since our results indicated that YAP1 and MRTF are activated in $Sox9^{High}/Sox10^{Low}$ BRAFi-resistant cells, we reasoned that pharmacologically targeting these transcriptional mechanisms would/might be sufficient to re-sensitize cells to vemurafenib. YAP1 is activated by YES1, a Src family kinase. Previous studies have used the Src family kinase inhibitor, dasatinib, to inhibit YES1 and subsequently inhibit YAP1 (49). To confirm this in the context of vemurafenib-resistant cells, we treated M229R and M238R cells with dasatinib and measured YAP1 nuclear localization. YAP1's nuclear localization is decreased in both cell lines upon dasatinib treatment **(Fig. 5A/B)**.

We next wanted to determine whether dasatinib re-sensitizes $Sox9^{High}/Sox10^{Low}$ BRAFi-resistant cells to Vemurafenib. Dasatinib treatment has only a minor effect on potentiating the vemurafenib response in the

parental UACC62P and M229P cells **(Fig. 5C/E)**. However, the vemurafenib response is greatly potentiated in the resistant UACC62R and M229R cells **(Fig. 5D/F)**. While UACC62R does not have as robust of YAP1 activation as M229R and M238R, the minor increase in YAP1 nuclear localization could explain why these cells also respond to dasatinib. This effect is consistent across all three $Sox9^{High}/Sox10^{Low}$ BRAFi-resistant cell lines **(Fig. 5K)**.

Our lab has developed a series of MRTF pathway inhibitors, including CCG-222740. We sought to determine whether this inhibitor can re-sensitize $Sox9^{High}/Sox10^{Low}$ BRAFi-resistant cells to Vemurafenib. CCG-22740 has only a modest effect on re-sensitizing M229R or M238R cells, which show strong YAP1 but low MRTF-A activation **(Fig. 5I/J/L)**. Interestingly, CCG-222740 re-sensitizes UACC62R cells **(Fig. 5G/H/L)** which was the only BRAFi-resistant cell line with strong nuclear localization of MRTF-A. This highlights the selectivity of CCG-222740 and the role of MRTF-A in BRAFi resistance. Taken together, these data demonstrate that inhibition of RhoA-regulated gene transcription in $Sox9^{High}/Sox10^{Low}$ cells, which can be mediated either by YAP or MRTF, re-sensitizes the melanoma cells to vemurafenib.

Discussion: In this study we sought to identify pharmacological "Achilles heels" for BRAFi-resistant melanoma cells/tumors. In theory, if pathway-centric dependences can be identified for cells with acquired resistance, then co-targeting these resistance pathways concurrently with MAPK pathway inhibitors may delay, prevent, or reverse resistance. We found evidence for Rho pathway activation in approximately half of BRAFi/MEKi-resistant human melanoma cells and tumors. In isogenic BRAFi-resistant cell lines, Rho pathway activation was accompanied by both an increase in actin stress fibers and MLC2 phosphorylation. These findings are consistent with previous reports which demonstrate that actin stress fibers are increased in cell line models of acquired BRAFi resistance (25). Building off these findings, we demonstrated that ROCK inhibition re-sensitizes Rho^{High} BRAFi-resistant cells to vemurafenib, highlighting the importance of this signaling pathway in adaptive BRAFi resistance. This finding also supports our bioinformatics predictions, since two ROCK inhibitors were among the drugs predicted to be most selective for $Sox10^{Low}$ melanoma tumors.

We next wanted to identify signaling mechanisms which are associated with Rho pathway activation. These signaling mechanisms could serve as biomarkers for Rho activation or these pathways could directly promote Rho activation. To this end, we analyzed UACC62P/R cells by RNA-seq. Upon acquisition of BRAFi-resistance, UACC62 cells lose expression of several melanocyte lineage genes such as TYR, MLANA, and SOX10, and gain expression of cancer invasion-associated genes including AXL and SOX9 as well as several collagen and integrin isoforms. Previous reports demonstrate that a switch in MITF/AXL gene expression levels mark BRAFi resistance (6, 46, 50), but we only observed minor changes in MITF expression by either RNA-seq, or qRTPCR (data not shown). Both MITF and Sox10 are critical for melanocyte pigmentation, and Sox10 regulates MITF expression (51, 52). Sox10 loss has also been demonstrated to promote BRAFi resistance in melanoma through a TGFβ-dependent mechanism (43). Since TGFβ signaling is a well-established activator of the Rho pathway (44, 45), we wanted to determine whether there was an association between Sox10 and RhoA in melanoma. All three of the $RhoA^{High}$ BRAFi-resistant cell lines have ~1000-fold downregulation of Sox10. And Sox10 is also inversely correlated with a RhoA/C signature in both bulk human melanoma tumors and single cells isolated from human melanoma tumors. These data demonstrate that Rho activation is associated with Sox10 loss. It will be important to determine whether Sox10 loss directly promotes RhoA activation or if it is part of a larger cell state transition that also includes RhoA activation.

As a result of modulating the actin cytoskeleton, Rho regulates gene transcription. Rho-induced F-actin polymerization allows for MRTF and YAP1 to translocate into the nucleus where they subsequently regulate gene transcription (30-34, 53). MRTF and YAP1 regulate similar suites of genes and function redundantly in many contexts. Interestingly, some reports suggest that MRTF and YAP1 physically interact and are present in close proximity on similar gene promoters (47), while others suggest more indirect mechanisms of shared gene expression control (48). While YAP1 has been previously demonstrated to promote BRAFi resistance in melanoma (7, 25, 37, 38), the role of MRTF in BRAFi resistance is unknown. In this study we demonstrate that nuclear accumulation of either MRTF-A or YAP1 is increased in $RhoA^{High}$ BRAFi-resistant cells. We also demonstrate that pharmacologically inhibiting either MRTF- or YAP1-mediated gene transcription re-sensitizes

BRAFi-resistant cells to vemurafenib. Further work is required to determine the nature of how MRTF promotes BRAFi resistance and whether those signaling mechanisms are similar to the mechanisms by which YAP1 promotes BRAFi resistance. Interestingly, we observed YAP1 activation in 2 of 3 RhoA^{High} resistant cell lines, and MRTF-A activation in the 3rd cell line. This may suggest that MRTF-A and YAP1 are acting redundantly in this context and that activation of either MRTF-A or YAP1 is sufficient to promote drug resistance.

This study demonstrates that Rho^{High} BRAFi-resistant cells are re-sensitized to vemurafenib by ROCK inhibitors and that this Rho^{High} phenotype is linked to a decrease in the expression of several melanocyte lineage genes, including Sox10. The direct signaling mechanisms which lead to Rho activation in melanoma cells are still unclear, but it is enticing to suggest that induction of TGFβ upon Sox10 loss may lead to Rho activation. Future studies will be necessary to elucidate details of these signaling networks. While it is already known that YAP1 promotes BRAFi resistance, these studies build upon that knowledge to demonstrate that dasatinib blocks the nuclear accumulation of YAP1 in BRAFi-resistant cells. Since dasatinib is already FDA-approved for other indications, it highlights the potential of re-purposing this drug for the treatment of BRAFi/MEKi-resistant melanoma. These studies also link MRTF-A activation to BRAFi resistance for the first time, highlighting the potential of targeting MRTF-mediated transcription to prevent or treat drug resistant melanoma. In total, these studies provide robust predictions of precision therapy approaches to prevent or treat clinical BRAFi resistance based on pharmacological inhibition of RhoA-mediated gene transcription.

1. Hodis E, Watson IR, Kryukov GV, Arold ST, Imielinski M, Theurillat JP, Nickerson E, Auclair D, Li L, Place C, Dicara D, Ramos AH, Lawrence MS, Cibulskis K, Sivachenko A, Voet D, Saksena G, Stransky N, Onofrio RC, Winckler W, Ardlie K, Wagle N, Wargo J, Chong K, Morton DL, Stemke-Hale K, Chen G, Noble M, Meyerson M, Ladbury JE, Davies MA, Gershenwald JE, Wagner SN, Hoon DS, Schadendorf D, Lander ES, Gabriel SB, Getz G, Garraway LA, Chin L. A landscape of driver mutations in melanoma. Cell. 2012;150(2):251-63. doi: 10.1016/j.cell.2012.06.024. PubMed PMID: 22817889; PMCID: PMC3600117.
2. Chapman PB, Hauschild A, Robert C, Haanen JB, Ascierto P, Larkin J, Dummer R, Garbe C, Testori A, Maio M, Hogg D, Lorigan P, Lebbe C, Jouary T, Schadendorf D, Ribas A, O'Day SJ, Sosman JA, Kirkwood JM, Eggermont AM, Dreno B, Nolop K, Li J, Nelson B, Hou J, Lee RJ, Flaherty KT, McArthur GA, Group B-S. Improved survival with vemurafenib in melanoma with BRAF V600E mutation. N Engl J Med. 2011;364(26):2507-16. doi: 10.1056/NEJMoa1103782. PubMed PMID: 21639808; PMCID: PMC3549296.
3. Larkin J, Ascierto PA, Dreno B, Atkinson V, Liszkay G, Maio M, Mandala M, Demidov L, Stroyakovskiy D, Thomas L, de la Cruz-Merino L, Dutriaux C, Garbe C, Sovak MA, Chang I, Choong N, Hack SP, McArthur GA, Ribas A. Combined vemurafenib and cobimetinib in BRAF-mutated melanoma. N Engl J Med. 2014;371(20):1867-76. doi: 10.1056/NEJMoa1408868. PubMed PMID: 25265494.
4. Robert C, Karaszewska B, Schachter J, Rutkowski P, Mackiewicz A, Stroiakovski D, Lichinitser M, Dummer R, Grange F, Mortier L, Chiarion-Sileni V, Drucis K, Krajsova I, Hauschild A, Lorigan P, Wolter P, Long GV, Flaherty K, Nathan P, Ribas A, Martin AM, Sun P, Crist W, Legos J, Rubin SD, Little SM, Schadendorf D. Improved overall survival in melanoma with combined dabrafenib and trametinib. N Engl J Med. 2015;372(1):30-9. doi: 10.1056/NEJMoa1412690. PubMed PMID: 25399551.
5. Johnson DB, Menzies AM, Zimmer L, Eroglu Z, Ye F, Zhao S, Rizos H, Sucker A, Scolyer RA, Gutzmer R, Gogas H, Kefford RF, Thompson JF, Becker JC, Berking C, Egberts F, Loquai C, Goldinger SM, Pupo GM, Hugo W, Kong X, Garraway LA, Sosman JA, Ribas A, Lo RS, Long GV, Schadendorf D. Acquired BRAF inhibitor resistance: A multicenter meta-analysis of the spectrum and frequencies, clinical behaviour, and phenotypic associations of resistance mechanisms. Eur J Cancer. 2015;51(18):2792-9. doi: 10.1016/j.ejca.2015.08.022. PubMed PMID: 26608120; PMCID: PMC4666799.
6. Song C, Piva M, Sun L, Hong A, Moriceau G, Kong X, Zhang H, Lomeli S, Qian J, Yu CC, Damoiseaux R, Kelley MC, Dahlman KB, Scumpia PO, Sosman JA, Johnson DB, Ribas A, Hugo W, Lo RS. Recurrent Tumor Cell-Intrinsic and -Extrinsic Alterations during MAPKi-Induced Melanoma Regression and Early Adaptation. Cancer Discov. 2017;7(11):1248-65. doi: 10.1158/2159-8290.CD-17-0401. PubMed PMID: 28864476.
7. Hugo W, Shi H, Sun L, Piva M, Song C, Kong X, Moriceau G, Hong A, Dahlman KB, Johnson DB, Sosman JA, Ribas A, Lo RS. Non-genomic and Immune Evolution of Melanoma Acquiring MAPKi Resistance. Cell. 2015;162(6):1271-85. doi: 10.1016/j.cell.2015.07.061. PubMed PMID: 26359985; PMCID: PMC4821508.
8. Nazarian R, Shi H, Wang Q, Kong X, Koya RC, Lee H, Chen Z, Lee MK, Attar N, Sazegar H, Chodon T, Nelson SF, McArthur G, Sosman JA, Ribas A, Lo RS. Melanomas acquire resistance to B-RAF(V600E) inhibition by RTK or N-RAS upregulation. Nature. 2010;468(7326):973-7. doi: 10.1038/nature09626. PubMed PMID: 21107323; PMCID: PMC3143360.
9. Van Allen EM, Wagle N, Sucker A, Treacy DJ, Johannessen CM, Goetz EM, Place CS, Taylor-Weiner A, Whittaker S, Kryukov GV, Hodis E, Rosenberg M, McKenna A, Cibulskis K, Farlow D, Zimmer L, Hillen U, Gutzmer R, Goldinger SM, Ugurel S, Gogas HJ, Egberts F, Berking C, Trefzer U, Loquai C, Weide B, Hassel JC, Gabriel SB, Carter SL, Getz G, Garraway LA, Schadendorf D, Dermatologic Cooperative Oncology Group of G. The genetic landscape of clinical resistance to RAF inhibition in metastatic melanoma. Cancer Discov. 2014;4(1):94-109. doi: 10.1158/2159-8290.CD-13-0617. PubMed PMID: 24265153; PMCID: PMC3947264.
10. Shi H, Moriceau G, Kong X, Lee MK, Lee H, Koya RC, Ng C, Chodon T, Scolyer RA, Dahlman KB, Sosman JA, Kefford RF, Long GV, Nelson SF, Ribas A, Lo RS. Melanoma whole-exome sequencing identifies (V600E)B-RAF amplification-mediated acquired B-RAF inhibitor resistance. Nat Commun. 2012;3:724. doi: 10.1038/ncomms1727. PubMed PMID: 22395615; PMCID: PMC3530385.

11. Poulikakos PI, Persaud Y, Janakiraman M, Kong X, Ng C, Moriceau G, Shi H, Atefi M, Titz B, Gabay MT, Salton M, Dahlman KB, Tadi M, Wargo JA, Flaherty KT, Kelley MC, Misteli T, Chapman PB, Sosman JA, Graeber TG, Ribas A, Lo RS, Rosen N, Solit DB. RAF inhibitor resistance is mediated by dimerization of aberrantly spliced BRAF(V600E). Nature. 2011;480(7377):387-90. doi: 10.1038/nature10662. PubMed PMID: 22113612; PMCID: PMC3266695.
12. Shi H, Hugo W, Kong X, Hong A, Koya RC, Moriceau G, Chodon T, Guo R, Johnson DB, Dahlman KB, Kelley MC, Kefford RF, Chmielowski B, Glaspy JA, Sosman JA, van Baren N, Long GV, Ribas A, Lo RS. Acquired resistance and clonal evolution in melanoma during BRAF inhibitor therapy. Cancer Discov. 2014;4(1):80-93. doi: 10.1158/2159-8290.CD-13-0642. PubMed PMID: 24265155; PMCID: PMC3936420.
13. Shaffer SM, Dunagin MC, Torborg SR, Torre EA, Emert B, Krepler C, Beqiri M, Sproesser K, Brafford PA, Xiao M, Eggan E, Anastopoulos IN, Vargas-Garcia CA, Singh A, Nathanson KL, Herlyn M, Raj A. Rare cell variability and drug-induced reprogramming as a mode of cancer drug resistance. Nature. 2017;546(7658):431-5. doi: 10.1038/nature22794. PubMed PMID: 28607484; PMCID: PMC5542814.
14. Das Thakur M, Salangsang F, Landman AS, Sellers WR, Pryer NK, Levesque MP, Dummer R, McMahon M, Stuart DD. Modelling vemurafenib resistance in melanoma reveals a strategy to forestall drug resistance. Nature. 2013;494(7436):251-5. doi: 10.1038/nature11814. PubMed PMID: 23302800; PMCID: PMC3930354.
15. Hong A, Moriceau G, Sun L, Lomeli S, Piva M, Damoiseaux R, Holmen SL, Sharpless NE, Hugo W, Lo RS. Exploiting Drug Addiction Mechanisms to Select against MAPKi-Resistant Melanoma. Cancer Discov. 2018;8(1):74-93. doi: 10.1158/2159-8290.CD-17-0682. PubMed PMID: 28923912.
16. Moriceau G, Hugo W, Hong A, Shi H, Kong X, Yu CC, Koya RC, Samatar AA, Khanlou N, Braun J, Ruchalski K, Seifert H, Larkin J, Dahlman KB, Johnson DB, Algazi A, Sosman JA, Ribas A, Lo RS. Tunable-combinatorial mechanisms of acquired resistance limit the efficacy of BRAF/MEK cotargeting but result in melanoma drug addiction. Cancer Cell. 2015;27(2):240-56. doi: 10.1016/j.ccell.2014.11.018. PubMed PMID: 25600339; PMCID: PMC4326539.
17. Klein RM, Higgins PJ. A switch in RND3-RHOA signaling is critical for melanoma cell invasion following mutant-BRAF inhibition. Mol Cancer. 2011;10:114. doi: 10.1186/1476-4598-10-114. PubMed PMID: 21917148; PMCID: PMC3180434.
18. Clark EA, Golub TR, Lander ES, Hynes RO. Genomic analysis of metastasis reveals an essential role for RhoC. Nature. 2000;406(6795):532-5. doi: 10.1038/35020106. PubMed PMID: 10952316.
19. Ruth MC, Xu Y, Maxwell IH, Ahn NG, Norris DA, Shellman YG. RhoC promotes human melanoma invasion in a PI3K/Akt-dependent pathway. J Invest Dermatol. 2006;126(4):862-8. doi: 10.1038/sj.jid.5700211. PubMed PMID: 16470169.
20. Routhier A, Astuccio M, Lahey D, Monfredo N, Johnson A, Callahan W, Partington A, Fellows K, Ouellette L, Zhidro S, Goodrow C, Smith A, Sullivan K, Simone P, Le L, Vezuli B, Zohni M, West E, Gleason D, Bryan B. Pharmacological inhibition of Rho-kinase signaling with Y-27632 blocks melanoma tumor growth. Oncol Rep. 2010;23(3):861-7. PubMed PMID: 20127030.
21. Delmas A, Cherier J, Pohorecka M, Medale-Giamarchi C, Meyer N, Casanova A, Sordet O, Lamant L, Savina A, Pradines A, Favre G. The c-Jun/RHOB/AKT pathway confers resistance of BRAF-mutant melanoma cells to MAPK inhibitors. Oncotarget. 2015;6(17):15250-64. doi: 10.18632/oncotarget.3888. PubMed PMID: 26098773; PMCID: PMC4558149.
22. Sit ST, Manser E. Rho GTPases and their role in organizing the actin cytoskeleton. J Cell Sci. 2011;124(Pt 5):679-83. doi: 10.1242/jcs.064964. PubMed PMID: 21321325.
23. Spiering D, Hodgson L. Dynamics of the Rho-family small GTPases in actin regulation and motility. Cell Adh Migr. 2011;5(2):170-80. PubMed PMID: 21178402; PMCID: PMC3084983.
24. Hodge RG, Ridley AJ. Regulating Rho GTPases and their regulators. Nat Rev Mol Cell Biol. 2016;17(8):496-510. doi: 10.1038/nrm.2016.67. PubMed PMID: 27301673.
25. Kim MH, Kim J, Hong H, Lee SH, Lee JK, Jung E, Kim J. Actin remodeling confers BRAF inhibitor resistance to melanoma cells through YAP/TAZ activation. EMBO J. 2016;35(5):462-78. doi: 10.15252/embj.201592081. PubMed PMID: 26668268; PMCID: PMC4772854.
26. Medjkane S, Perez-Sanchez C, Gaggioli C, Sahai E, Treisman R. Myocardin-related transcription factors and SRF are required for cytoskeletal dynamics and experimental metastasis. Nat Cell Biol. 2009;11(3):257-68. doi: 10.1038/ncb1833. PubMed PMID: 19198601.

27. Bell JL, Haak AJ, Wade SM, Kirchhoff PD, Neubig RR, Larsen SD. Optimization of novel nipecotic bis(amide) inhibitors of the Rho/MKL1/SRF transcriptional pathway as potential anti-metastasis agents. Bioorg Med Chem Lett. 2013;23(13):3826-32. doi: 10.1016/j.bmcl.2013.04.080. PubMed PMID: 23707258; PMCID: PMC3707396.
28. Haak AJ, Appleton KM, Lisabeth EM, Misek S, Ji Y, Wade SM, Bell JL, Rockwell CE, Airik M, Krook MA, Larsen SD, Verhaegen ME, Lawlor ER, Neubig RR. Pharmacological inhibition of Myocardin-related transcription factor pathway blocks lung metastases of RhoC overexpressing melanoma. Mol Cancer Ther. 2016. doi: 10.1158/1535-7163.MCT-16-0482. PubMed PMID: 27837031.
29. Hutchings KM, Lisabeth EM, Rajeswaran W, Wilson MW, Sorenson RJ, Campbell PL, Ruth JH, Amin A, Tsou PS, Leipprandt JR, Olson SR, Wen B, Zhao T, Sun D, Khanna D, Fox DA, Neubig RR, Larsen SD. Pharmacokinetic optimitzation of CCG-203971: Novel inhibitors of the Rho/MRTF/SRF transcriptional pathway as potential antifibrotic therapeutics for systemic scleroderma. Bioorg Med Chem Lett. 2017;27(8):1744-9. doi: 10.1016/j.bmcl.2017.02.070. PubMed PMID: 28285914; PMCID: PMC5395305.
30. Esnault C, Stewart A, Gualdrini F, East P, Horswell S, Matthews N, Treisman R. Rho-actin signaling to the MRTF coactivators dominates the immediate transcriptional response to serum in fibroblasts. Genes Dev. 2014;28(9):943-58. doi: 10.1101/gad.239327.114. PubMed PMID: 24732378; PMCID: PMC4018493.
31. Mouilleron S, Guettler S, Langer CA, Treisman R, McDonald NQ. Molecular basis for G-actin binding to RPEL motifs from the serum response factor coactivator MAL. EMBO J. 2008;27(23):3198-208. doi: 10.1038/emboj.2008.235. PubMed PMID: 19008859; PMCID: PMC2583105.
32. Mouilleron S, Langer CA, Guettler S, McDonald NQ, Treisman R. Structure of a pentavalent G-actin*MRTF-A complex reveals how G-actin controls nucleocytoplasmic shuttling of a transcriptional coactivator. Sci Signal. 2011;4(177):ra40. doi: 10.1126/scisignal.2001750. PubMed PMID: 21673315.
33. Posern G, Treisman R. Actin' together: serum response factor, its cofactors and the link to signal transduction. Trends Cell Biol. 2006;16(11):588-96. doi: 10.1016/j.tcb.2006.09.008. PubMed PMID: 17035020.
34. Seo J, Kim J. Regulation of Hippo signaling by actin remodeling. BMB Rep. 2018;51(3):151-6. PubMed PMID: 29353600; PMCID: PMC5882222.
35. Mana-Capelli S, Paramasivam M, Dutta S, McCollum D. Angiomotins link F-actin architecture to Hippo pathway signaling. Mol Biol Cell. 2014;25(10):1676-85. doi: 10.1091/mbc.E13-11-0701. PubMed PMID: 24648494; PMCID: PMC4019498.
36. Dai X, She P, Chi F, Feng Y, Liu H, Jin D, Zhao Y, Guo X, Jiang D, Guan KL, Zhong TP, Zhao B. Phosphorylation of angiomotin by Lats1/2 kinases inhibits F-actin binding, cell migration, and angiogenesis. J Biol Chem. 2013;288(47):34041-51. doi: 10.1074/jbc.M113.518019. PubMed PMID: 24106267; PMCID: PMC3837143.
37. Lin L, Sabnis AJ, Chan E, Olivas V, Cade L, Pazarentzos E, Asthana S, Neel D, Yan JJ, Lu X, Pham L, Wang MM, Karachaliou N, Cao MG, Manzano JL, Ramirez JL, Torres JM, Buttitta F, Rudin CM, Collisson EA, Algazi A, Robinson E, Osman I, Munoz-Couselo E, Cortes J, Frederick DT, Cooper ZA, McMahon M, Marchetti A, Rosell R, Flaherty KT, Wargo JA, Bivona TG. The Hippo effector YAP promotes resistance to RAF- and MEK-targeted cancer therapies. Nat Genet. 2015;47(3):250-6. doi: 10.1038/ng.3218. PubMed PMID: 25665005; PMCID: PMC4930244.
38. Fisher ML, Grun D, Adhikary G, Xu W, Eckert RL. Inhibition of YAP function overcomes BRAF inhibitor resistance in melanoma cancer stem cells. Oncotarget. 2017;8(66):110257-72. doi: 10.18632/oncotarget.22628. PubMed PMID: 29299145; PMCID: PMC5746380.
39. Harris ML, Baxter LL, Loftus SK, Pavan WJ. Sox proteins in melanocyte development and melanoma. Pigment Cell Melanoma Res. 2010;23(4):496-513. doi: 10.1111/j.1755-148X.2010.00711.x. PubMed PMID: 20444197; PMCID: PMC2906668.
40. Mohamed A, Gonzalez RS, Lawson D, Wang J, Cohen C. SOX10 expression in malignant melanoma, carcinoma, and normal tissues. Appl Immunohistochem Mol Morphol. 2013;21(6):506-10. doi: 10.1097/PAI.0b013e318279bc0a. PubMed PMID: 23197006.
41. Shakhova O, Cheng P, Mishra PJ, Zingg D, Schaefer SM, Debbache J, Hausel J, Matter C, Guo T, Davis S, Meltzer P, Mihic-Probst D, Moch H, Wegner M, Merlino G, Levesque MP, Dummer R, Santoro R, Cinelli P, Sommer L. Antagonistic cross-regulation between Sox9 and Sox10 controls an anti-tumorigenic program in melanoma. PLoS Genet. 2015;11(1):e1004877. doi: 10.1371/journal.pgen.1004877. PubMed PMID: 25629959; PMCID: PMC4309598.
42. Tsherniak A, Vazquez F, Montgomery PG, Weir BA, Kryukov G, Cowley GS, Gill S, Harrington WF, Pantel S, Krill-Burger JM, Meyers RM, Ali L, Goodale A, Lee Y, Jiang G, Hsiao J, Gerath WFJ, Howell S, Merkel E, Ghandi M, Garraway LA,

Root DE, Golub TR, Boehm JS, Hahn WC. Defining a Cancer Dependency Map. Cell. 2017;170(3):564-76 e16. doi: 10.1016/j.cell.2017.06.010. PubMed PMID: 28753430; PMCID: PMC5667678.
43. Sun C, Wang L, Huang S, Heynen GJ, Prahallad A, Robert C, Haanen J, Blank C, Wesseling J, Willems SM, Zecchin D, Hobor S, Bajpe PK, Lieftink C, Mateus C, Vagner S, Grernrum W, Hofland I, Schlicker A, Wessels LF, Beijersbergen RL, Bardelli A, Di Nicolantonio F, Eggermont AM, Bernards R. Reversible and adaptive resistance to BRAF(V600E) inhibition in melanoma. Nature. 2014;508(7494):118-22. doi: 10.1038/nature13121. PubMed PMID: 24670642.
44. Rosman DS, Phukan S, Huang CC, Pasche B. TGFBR1*6A enhances the migration and invasion of MCF-7 breast cancer cells through RhoA activation. Cancer Res. 2008;68(5):1319-28. doi: 10.1158/0008-5472.CAN-07-5424. PubMed PMID: 18316594; PMCID: PMC2673101.
45. Bhowmick NA, Ghiassi M, Aakre M, Brown K, Singh V, Moses HL. TGF-beta-induced RhoA and p160ROCK activation is involved in the inhibition of Cdc25A with resultant cell-cycle arrest. Proc Natl Acad Sci U S A. 2003;100(26):15548-53. doi: 10.1073/pnas.2536483100. PubMed PMID: 14657354; PMCID: PMC307605.
46. Tirosh I, Izar B, Prakadan SM, Wadsworth MH, 2nd, Treacy D, Trombetta JJ, Rotem A, Rodman C, Lian C, Murphy G, Fallahi-Sichani M, Dutton-Regester K, Lin JR, Cohen O, Shah P, Lu D, Genshaft AS, Hughes TK, Ziegler CG, Kazer SW, Gaillard A, Kolb KE, Villani AC, Johannessen CM, Andreev AY, Van Allen EM, Bertagnolli M, Sorger PK, Sullivan RJ, Flaherty KT, Frederick DT, Jane-Valbuena J, Yoon CH, Rozenblatt-Rosen O, Shalek AK, Regev A, Garraway LA. Dissecting the multicellular ecosystem of metastatic melanoma by single-cell RNA-seq. Science. 2016;352(6282):189-96. doi: 10.1126/science.aad0501. PubMed PMID: 27124452; PMCID: PMC4944528.
47. Yu OM, Benitez JA, Plouffe SW, Ryback D, Klein A, Smith J, Greenbaum J, Delatte B, Rao A, Guan KL, Furnari FB, Chaim OM, Miyamoto S, Brown JH. YAP and MRTF-A, transcriptional co-activators of RhoA-mediated gene expression, are critical for glioblastoma tumorigenicity. Oncogene. 2018. doi: 10.1038/s41388-018-0301-5. PubMed PMID: 29887596.
48. Foster CT, Gualdrini F, Treisman R. Mutual dependence of the MRTF-SRF and YAP-TEAD pathways in cancer-associated fibroblasts is indirect and mediated by cytoskeletal dynamics. Genes Dev. 2017;31(23-24):2361-75. doi: 10.1101/gad.304501.117. PubMed PMID: 29317486; PMCID: PMC5795783.
49. Rosenbluh J, Nijhawan D, Cox AG, Li X, Neal JT, Schafer EJ, Zack TI, Wang X, Tsherniak A, Schinzel AC, Shao DD, Schumacher SE, Weir BA, Vazquez F, Cowley GS, Root DE, Mesirov JP, Beroukhim R, Kuo CJ, Goessling W, Hahn WC. beta-Catenin-driven cancers require a YAP1 transcriptional complex for survival and tumorigenesis. Cell. 2012;151(7):1457-73. doi: 10.1016/j.cell.2012.11.026. PubMed PMID: 23245941; PMCID: PMC3530160.
50. Konieczkowski DJ, Johannessen CM, Abudayyeh O, Kim JW, Cooper ZA, Piris A, Frederick DT, Barzily-Rokni M, Straussman R, Haq R, Fisher DE, Mesirov JP, Hahn WC, Flaherty KT, Wargo JA, Tamayo P, Garraway LA. A melanoma cell state distinction influences sensitivity to MAPK pathway inhibitors. Cancer Discov. 2014;4(7):816-27. doi: 10.1158/2159-8290.CD-13-0424. PubMed PMID: 24771846; PMCID: PMC4154497.
51. Tudrej KB, Czepielewska E, Kozlowska-Wojciechowska M. SOX10-MITF pathway activity in melanoma cells. Arch Med Sci. 2017;13(6):1493-503. doi: 10.5114/aoms.2016.60655. PubMed PMID: 29181082; PMCID: PMC5701683.
52. Lee M, Goodall J, Verastegui C, Ballotti R, Goding CR. Direct regulation of the Microphthalmia promoter by Sox10 links Waardenburg-Shah syndrome (WS4)-associated hypopigmentation and deafness to WS2. J Biol Chem. 2000;275(48):37978-83. doi: 10.1074/jbc.M003816200. PubMed PMID: 10973953.
53. Si Y, Ji X, Cao X, Dai X, Xu L, Zhao H, Guo X, Yan H, Zhang H, Zhu C, Zhou Q, Tang M, Xia Z, Li L, Cong YS, Ye S, Liang TB, Feng XH, Zhao B. Src inhibits the Hippo tumor suppressor pathway through tyrosine phosphorylation of Lats1. Cancer Res. 2017. doi: 10.1158/0008-5472.CAN-17-0391. PubMed PMID: 28754671.

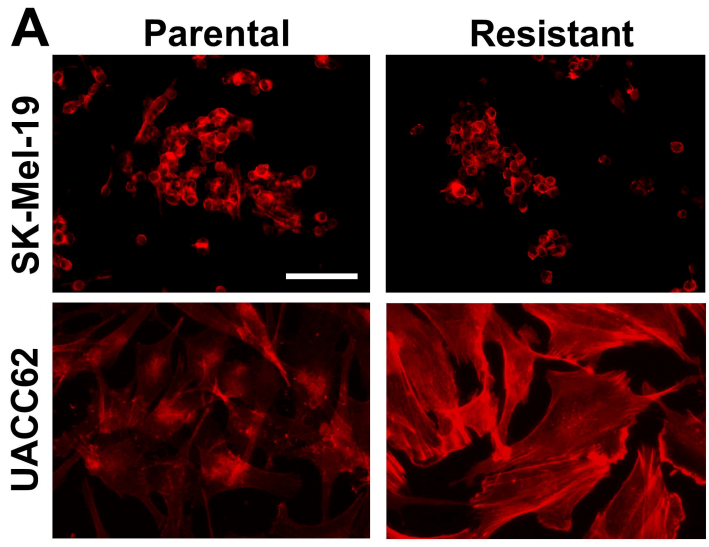
A
Parental
Resistant
SK-Mel-19
UACC62

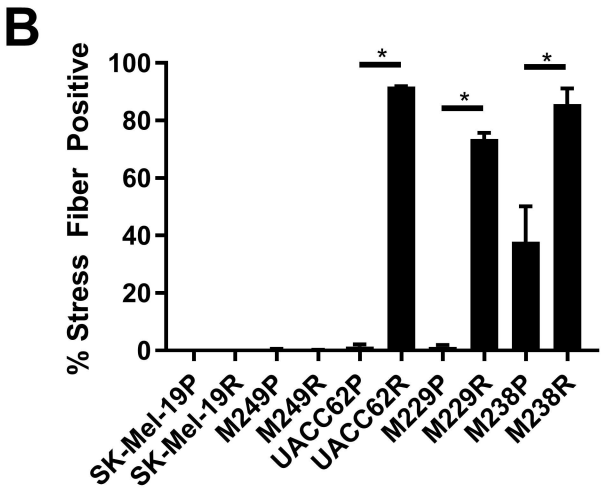
B
% Stress Fiber Positive
100
80
60
40
20
0
*
*
*
SK-Mel-19P
SK-Mel-19R
M249P
M249R
UACC62P
UACC62R
M229P
M229R
M238P
M238R

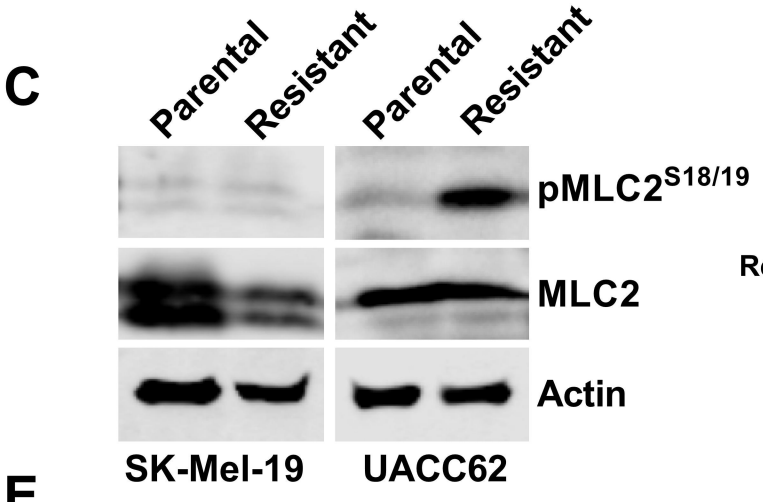
C
Parental
Resistant
Parental
Resistant
pMLC2S18/19
MLC2
Actin
SK-Mel-19
UACC62

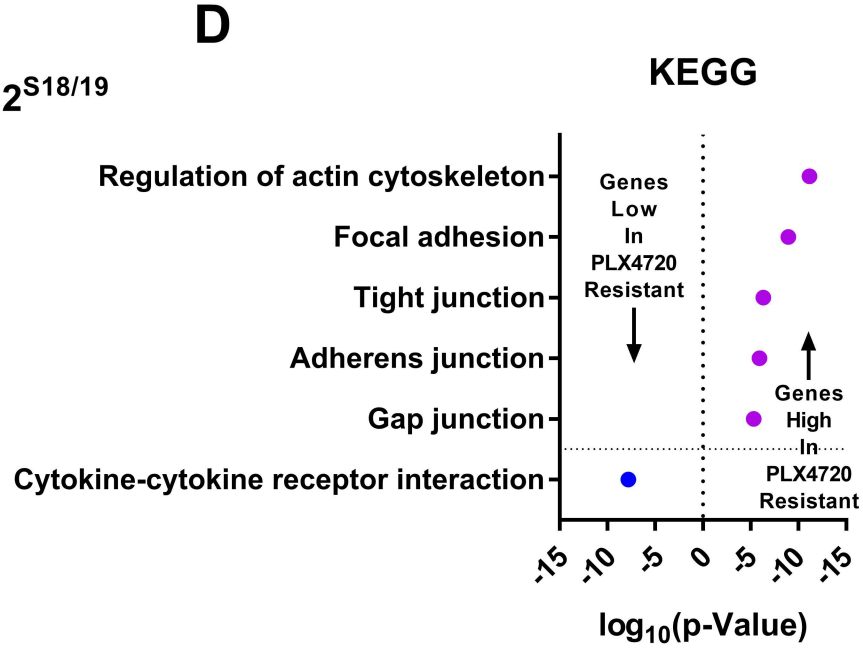
D
KEGG
Regulation of actin cytoskeleton
Focal adhesion
Tight junction
Adherens junction
Gap junction
Cytokine-cytokine receptor interaction
Genes Low In PLX4720 Resistant
Genes High In PLX4720 Resistant
-15
-10
-5
0
5
10
15
log10(p-Value)

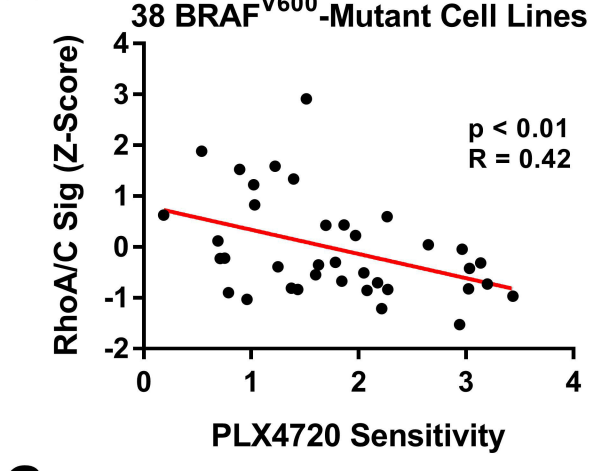
E
38 BRAFV600-Mutant Cell Lines
RhoA/C Sig (Z-Score)
p < 0.01
R = 0.42
PLX4720 Sensitivity

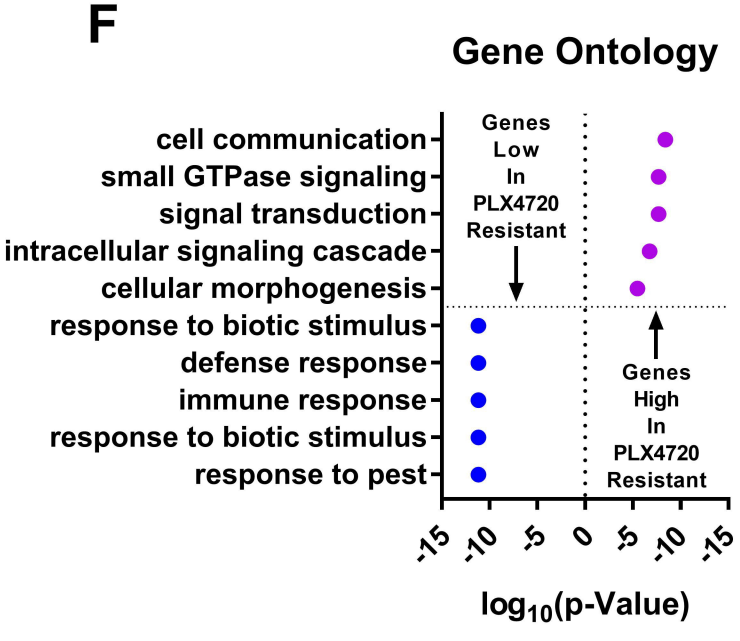
F
Gene Ontology
cell communication
small GTPase signaling
signal transduction
intracellular signaling cascade
cellular morphogenesis
response to biotic stimulus
defense response
immune response
response to biotic stimulus
response to pest
Genes Low In PLX4720 Resistant
Genes High In PLX4720 Resistant
-15
-10
-5
0
5
10
15
log10(p-Value)

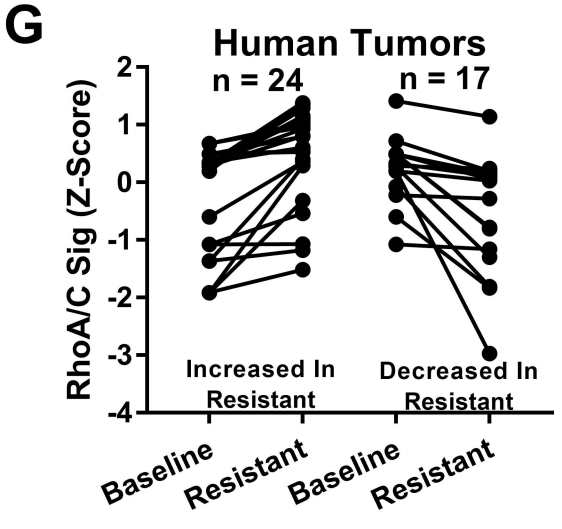
G
Human Tumors
n = 24
n = 17
RhoA/C Sig (Z-Score)
Increased In Resistant
Decreased In Resistant
Baseline
Resistant
Baseline
Resistant

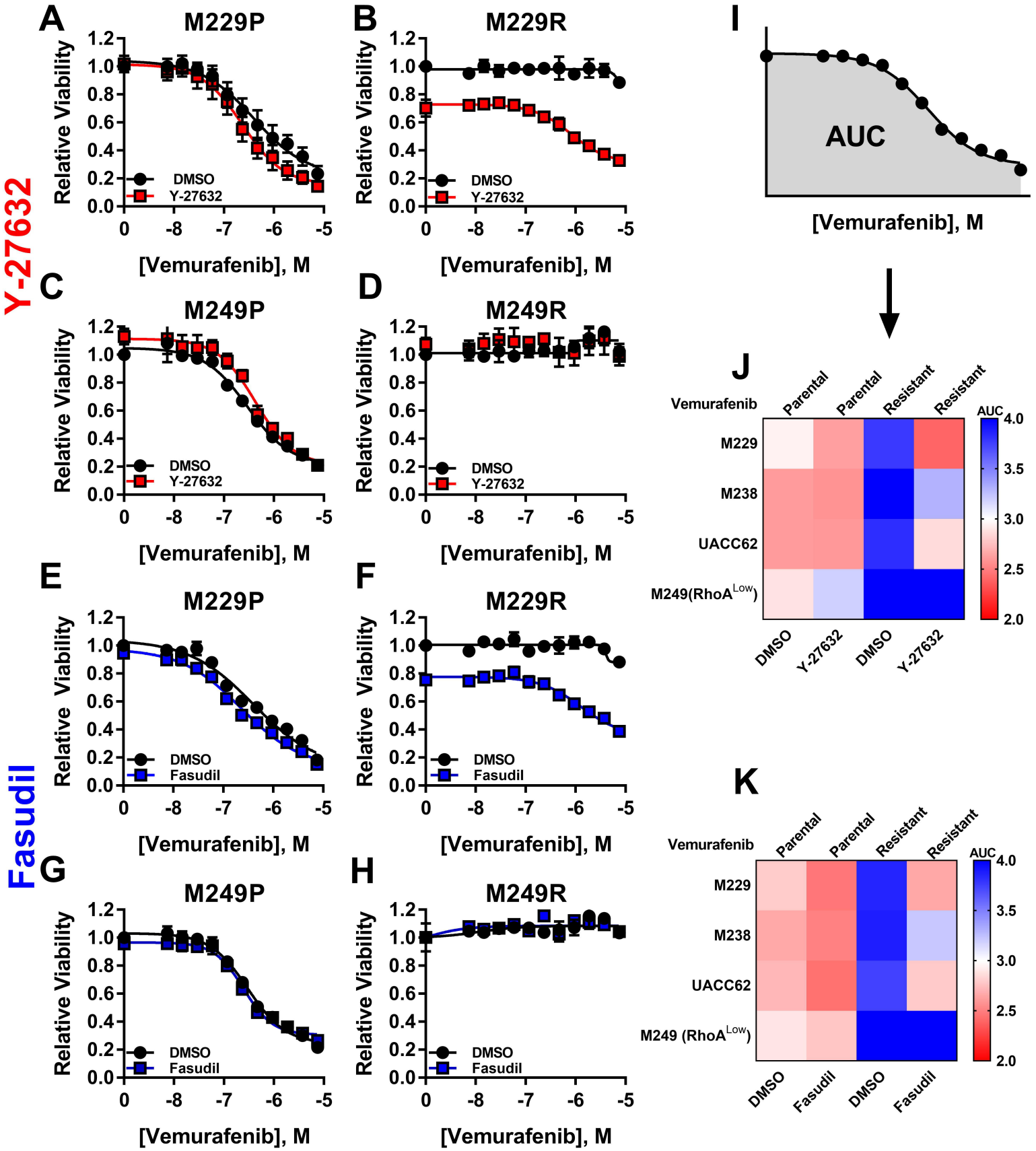
Y-27632
Fasudil
A
M229P
B
M229R
C
M249P
D
M249R
E
M229P
F
M229R
G
M249P
H
M249R
Relative Viability
[Vemurafenib], M
DMSO
Y-27632
Fasudil
I
AUC
[Vemurafenib], M
J
Vemurafenib
Parental
Parental
Resistant
Resistant
M229
M238
UACC62
M249(RhoA^Low)
DMSO
Y-27632
DMSO
Y-27632
AUC
K
Vemurafenib
Parental
Parental
Resistant
Resistant
M229
M238
UACC62
M249 (RhoA^Low)
DMSO
Fasudil
DMSO
Fasudil
AUC

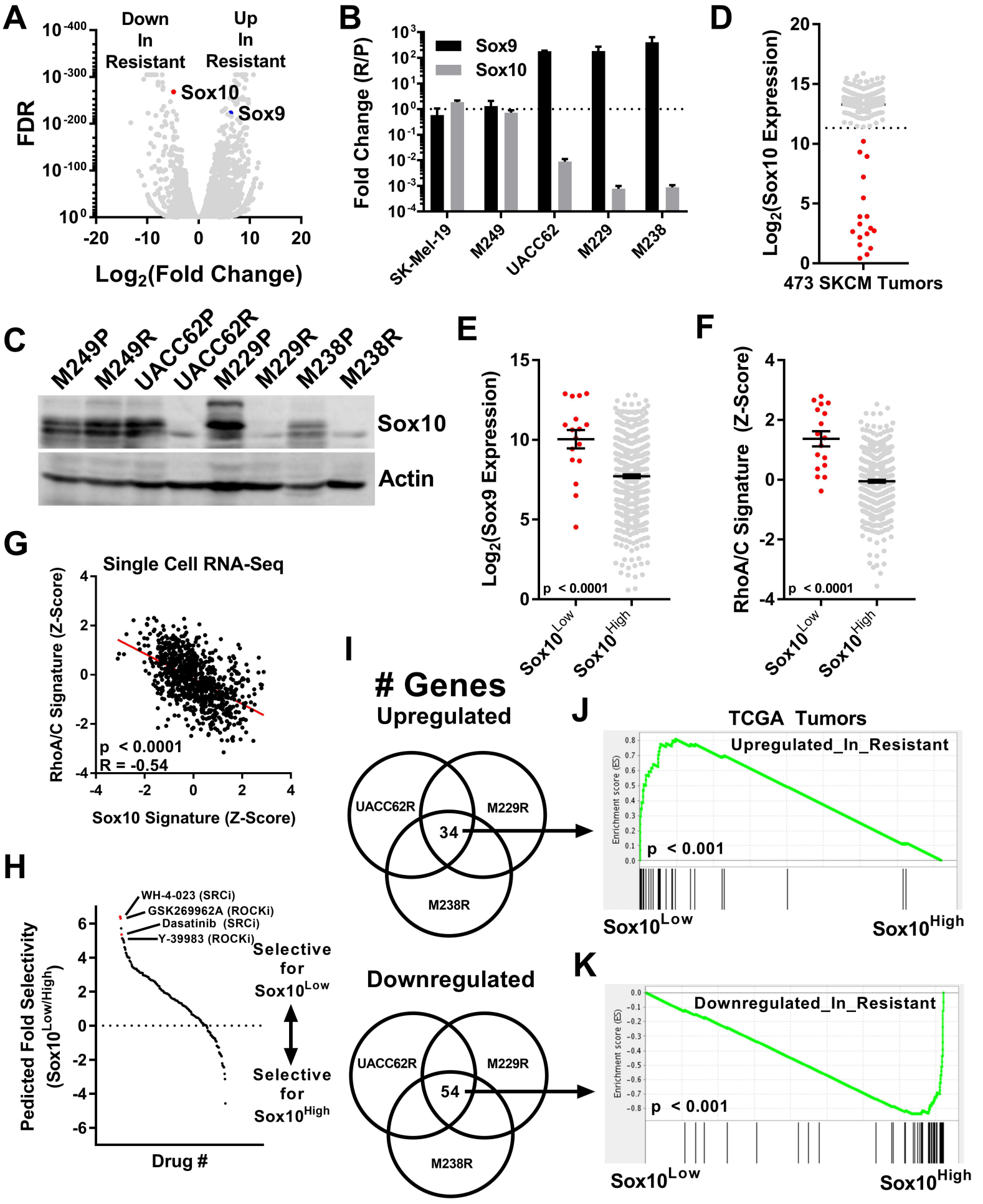
A
Down In Resistant
Up In Resistant
Sox10
Sox9
FDR
Log2(Fold Change)
B
Sox9
Sox10
Fold Change (R/P)
SK-Mel-19
M249
UACC62
M229
M238
D
Log2(Sox10 Expression)
473 SKCM Tumors
C
M249P
M249R
UACC62P
UACC62R
M229P
M229R
M238P
M238R
Sox10
Actin
E
Log2(Sox9 Expression)
p < 0.0001
Sox10Low
Sox10High
F
RhoA/C Signature (Z-Score)
p < 0.0001
Sox10Low
Sox10High
G
Single Cell RNA-Seq
RhoA/C Signature (Z-Score)
p < 0.0001
R = -0.54
Sox10 Signature (Z-Score)
H
WH-4-023 (SRCi)
GSK269962A (ROCKi)
Dasatinib (SRCi)
Y-39983 (ROCKi)
Selective for Sox10Low
Selective for Sox10High
Pedicted Fold Selectivity (Sox10Low/High)
Drug #
I
Genes
Upregulated
UACC62R
M229R
M238R
34
Downregulated
UACC62R
M229R
M238R
54
J
TCGA Tumors
Upregulated_In_Resistant
Enrichment score (ES)
p < 0.001
Sox10Low
Sox10High
K
Downregulated_In_Resistant
Enrichment score (ES)
p < 0.001
Sox10Low
Sox10High

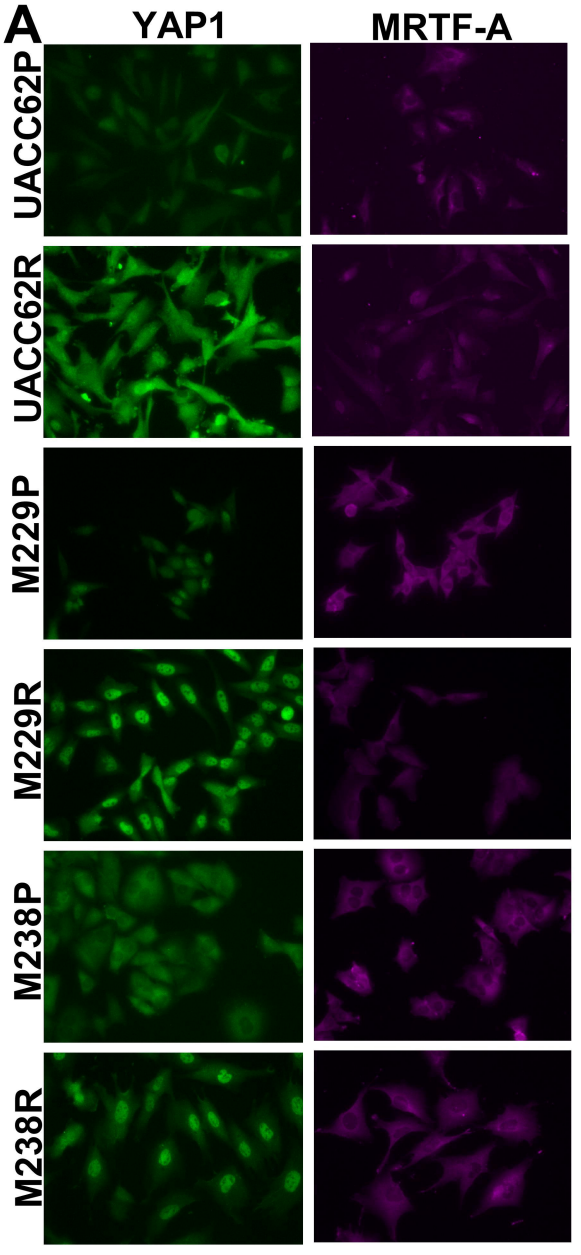
A
YAP1
MRTF-A
UACC62P
UACC62R
M229P
M229R
M238P
M238R

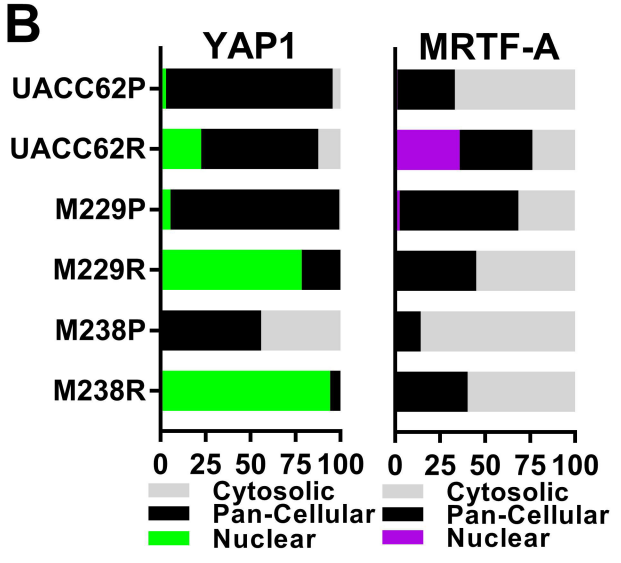
B
YAP1
MRTF-A
UACC62P
UACC62R
M229P
M229R
M238P
M238R
0 25 50 75 100
Cytosolic
Pan-Cellular
Nuclear

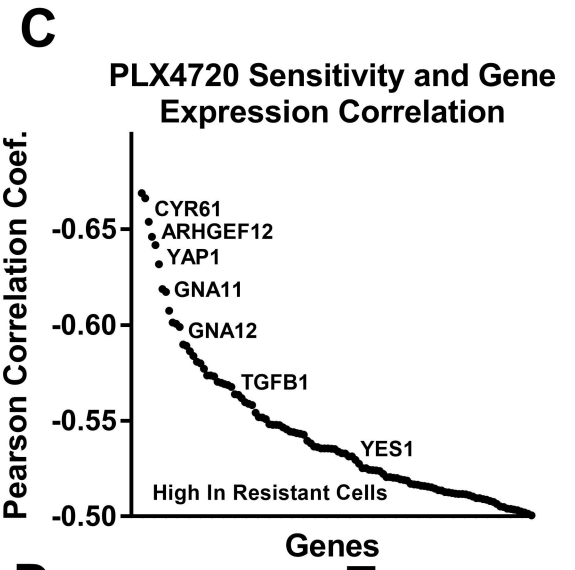
C
PLX4720 Sensitivity and Gene Expression Correlation
Pearson Correlation Coef.
-0.65
-0.60
-0.55
-0.50
CYR61
ARHGEF12
YAP1
GNA11
GNA12
TGFB1
YES1
High In Resistant Cells
Genes

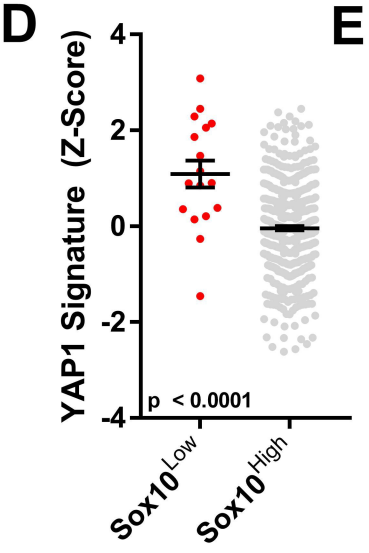
D
YAP1 Signature (Z-Score)
4
2
0
-2
-4
p < 0.0001
Sox10Low
Sox10High

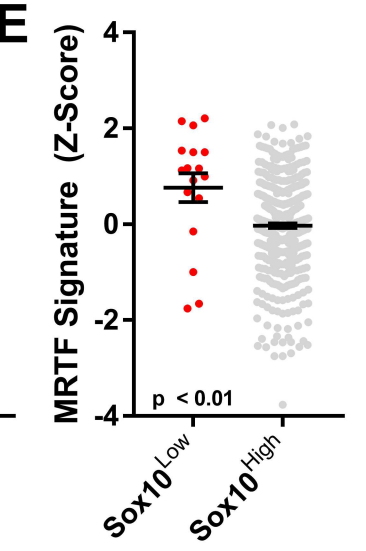
E
MRTF Signature (Z-Score)
4
2
0
-2
-4
p < 0.01
Sox10Low
Sox10High

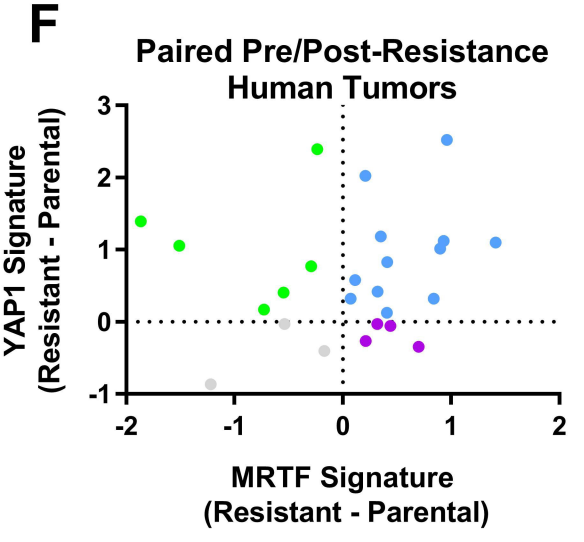
F
Paired Pre/Post-Resistance Human Tumors
YAP1 Signature (Resistant - Parental)
3
2
1
0
-1
-2
-1
0
1
2
MRTF Signature (Resistant - Parental)

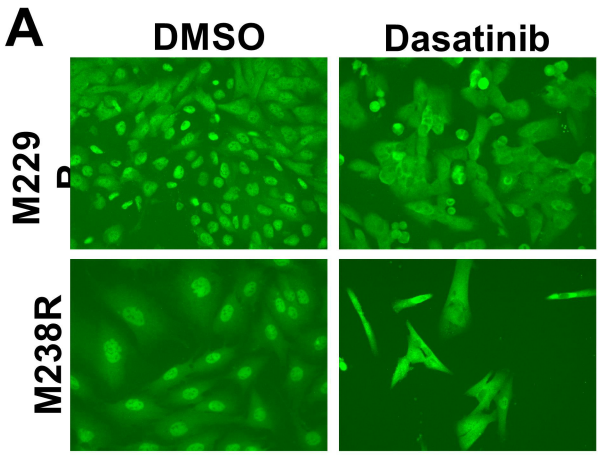
A
DMSO
Dasatinib
M229
M238R

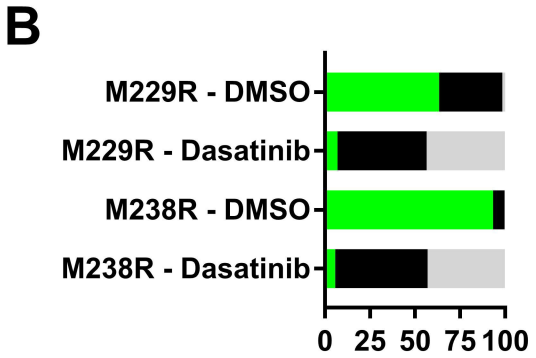
B
M229R - DMSO
M229R - Dasatinib
M238R - DMSO
M238R - Dasatinib
0
25
50
75
100

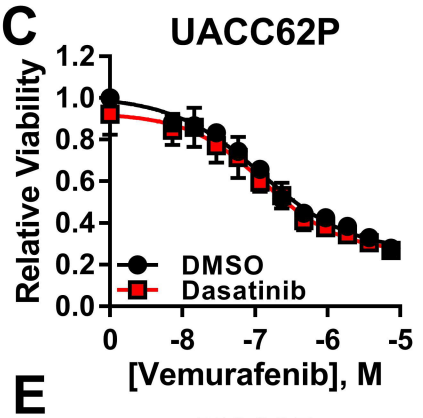
C
UACC62P
Relative Viability
DMSO
Dasatinib
[Vemurafenib], M

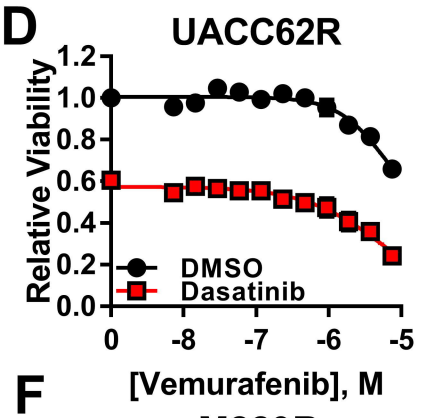
D
UACC62R
Relative Viability
DMSO
Dasatinib
[Vemurafenib], M

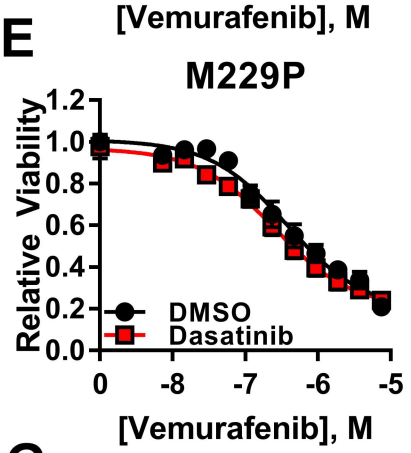
E
M229P
Relative Viability
DMSO
Dasatinib
[Vemurafenib], M

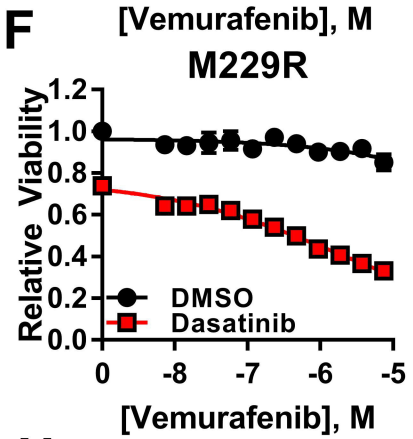
F
M229R
Relative Viability
DMSO
Dasatinib
[Vemurafenib], M

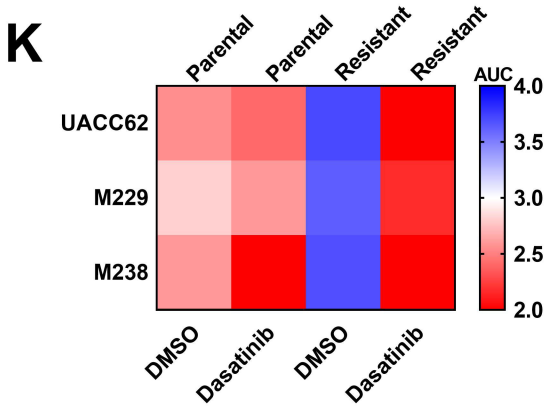
K
Parental
Parental
Resistant
Resistant
UACC62
M229
M238
DMSO
Dasatinib
DMSO
Dasatinib
AUC
4.0
3.5
3.0
2.5
2.0

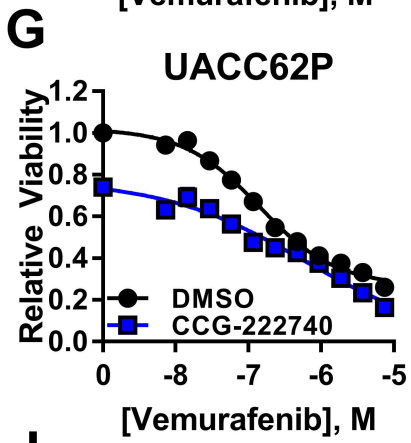
G
UACC62P
Relative Viability
DMSO
CCG-222740
[Vemurafenib], M

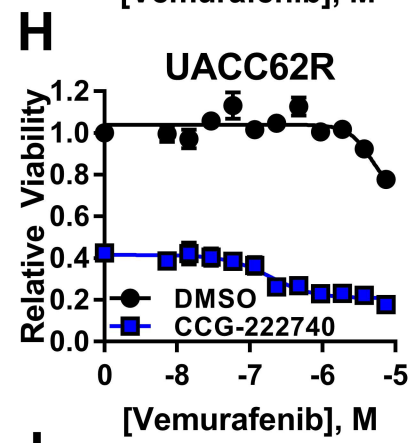
H
UACC62R
Relative Viability
DMSO
CCG-222740
[Vemurafenib], M

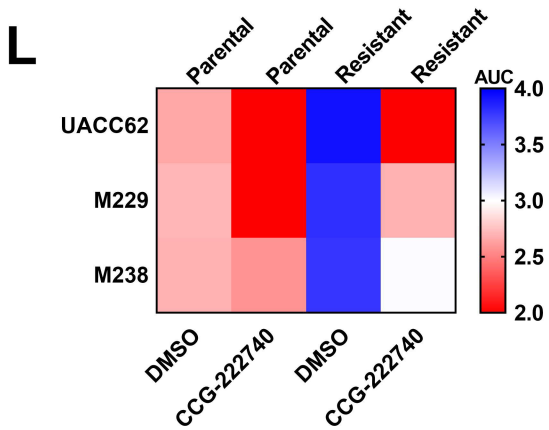
L
Parental
Parental
Resistant
Resistant
UACC62
M229
M238
DMSO
CCG-222740
DMSO
CCG-222740
AUC
4.0
3.5
3.0
2.5
2.0

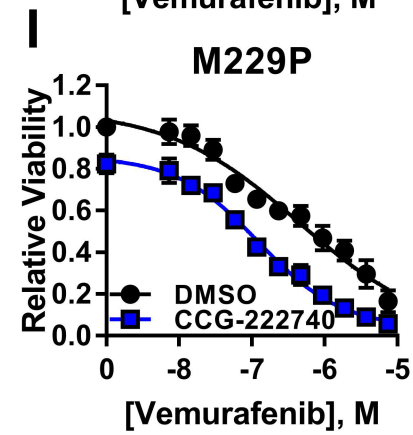
I
M229P
Relative Viability
DMSO
CCG-222740
[Vemurafenib], M

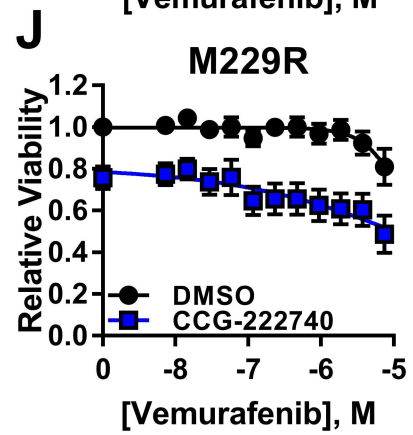
J
M229R
Relative Viability
DMSO
CCG-222740
[Vemurafenib], M